# Data Storage Report

## Tsunamis due to ice masses: Different calving mechanisms and linkage to landslide-tsunamis

Ice-tsunamis

Delta Basin, Stichting Deltares

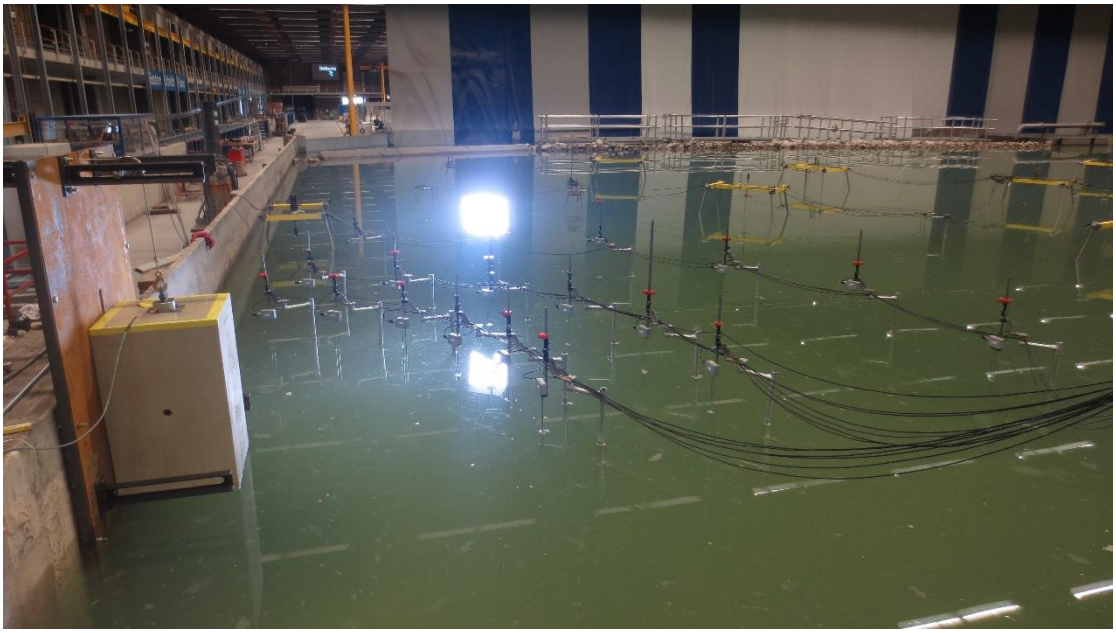

Author: Dr Valentin Heller, University of Nottingham

# Status form

## Document information

| | |
|---|---|
| **Project acronym** | Ice-tsunamis |
| **Provider** | Stichting Deltares |
| **Facility** | Delta Basin |
| **Title** | Tsunamis due to ice masses: Different calving mechanisms and linkage to landslide-tsunamis |
| **1st user group contact (name/email)** | Dr Valentin Heller, Valentin.heller@nottingham.ac.uk |
| **2nd user group contact (name/email)** | Mr Fan Chen, evxfc3@exmail.nottingham.ac.uk |
| **1st provider contact (name/email)** | Mr Mark Klein Breteler, Mark.KleinBreteler@deltares.nl |
| **2nd provider contact (name/email)** | Dr Guido Wolters, Guido.Wolters@deltares.nl |
| **Start date experiment (dd-mm-yyyy)** | 10-08-2017 |
| **End date experiment (dd-mm-yyyy)** | 01-09-2017 |

## Document history

| Date | Status | Author | Reviewer | Approver |
|---|---|---|---|---|
| 15-06-2017 | Draft | Dr Valentin Heller | [provider name] | |
| 04-09-2017 | Draft | Dr Valentin Heller | [provider name] | |
| 05-10-2017 | Final version 1 | Dr Valentin Heller | Dr Guido Wolters | |
| 12-10-2017 | Final version 1 | Dr Valentin Heller | Mark Klein Breteler | |
| 31-01-2019 | Final version 2 | Dr Valentin Heller | | |

## Document objective

This data storage plan describes the experimental program and how tests should be performed. When all data has been obtained, the data storage plan is updated to a data storage report. In the data storage report, the data is described so that others can use them.

## Acknowledgement

The work described in this publication was supported by the European Community's Horizon 2020 Research and Innovation Programme through the grant to HYDRALAB-PLUS, Contract no. 654110.

## Disclaimer

# Contents

# 1 Objectives

The background of this study can be found in Chen et al. (2019), Heller et al. (2019) and on the HYDRALAB+ website under *Experiments by Invited Researchers* under the main menu *Research & Resource* (search with the key phrase “Tsunami”). This research aims to enhance our physical understanding of tsunamis caused by ice calving and to support the associated “ice-tsunami” hazard assessment. This will be achieved with the following five objectives:

I. Conduct large-scale ice-tsunami experiments in the 50 m × 50 m large Delta Basin under variation of the ice calving mechanisms (capsizing, fall, over-turning) as well as the mass volume and kinematics

II. Quantify the tsunami features (height, length, velocity) and cross-compare the tsunamigenic potential from the five different ice calving mechanisms

III. Relate the new findings to an established landslide-tsunami hazard assessment method to potentially transfer knowledge

IV. Analysis of the new data using the highly promising new wave component decomposition method Korteweg-de Vries equations in combination with the nonlinear Fourier transform

V. Provide benchmark test cases to the numerical modelling community and apply the test cases to calibrate and validate numerical simulations of members of the project team to investigate additional ice-tsunami scenarios

# 2 Experimental setup

## 2.1 General description

Several ice calving mechanisms have been proposed in the technical literature including (i) capsizing, (ii) fall and (iii) over-turning (Fig. 2.1a). In mechanism (i) the ice mass is neutrally floating offshore such that gravity and buoyancy forces are in equilibrium. The behaviour of an ice mass in mechanisms (ii) and (iii) depends on the vertical position of the mass relative to the still water level (SWL); If the mass is initially located above the SWL, then gravity force is most relevant for the mechanism (gravity dominated) and the mass moves downwards after release. This is illustrated in the two sketches on the left-hand side of Figs. 2.1aii and 2.1aiii. If the mass is initially located below the SWL, then the buoyancy force is most relevant for the mechanism (buoyancy dominated) and the mass moves towards the water surface (sketches on the right-hand side of Figs. 2.1aii and 2.1aiii). In this study all five ice calving mechanisms have been investigated namely (i) capsizing, (ii) fall (gravity and buoyancy dominated) and (iii) over-turning (gravity and buoyancy dominated) and their tsunamigenic potential.

These five ice calving mechanisms were investigated in the 50 m × 50 m large Delta Basin (picture title page). Blocks consisting of Polypropylene Homopolymer (PPH) with a density similar to ice (≈920 kg/m$^3$) were released offshore (capsizing, Figs. 2.1b and 5.1c) and at the vertical boundary of the basin (fall, over-turning, Figs. 2.1c,d, 5.1a,b and picture title page). The block sizes were 0.800 m × 0.500 m × 0.500 m (block 1, picture title page) and 0.800 m × 0.500 m × 0.250 m (block 2, picture on bottom of Appendix A). These blocks were unstable in the initial positions due to an imbalance between gravity and buoyancy forces. Their movement was controlled with a rod allowing for rotation and vertical translation (capsizing), an electromagnet (fall) and a fixed rod defining the axis of rotation (over-turning). Some additional tests have been conducted with a 0.215 diameter sphere simulated by a basketball filled with water. Details of the experimental set-up for the individual ice calving mechanisms are given in Section 4 and Appendix B shows detailed technical drawings.

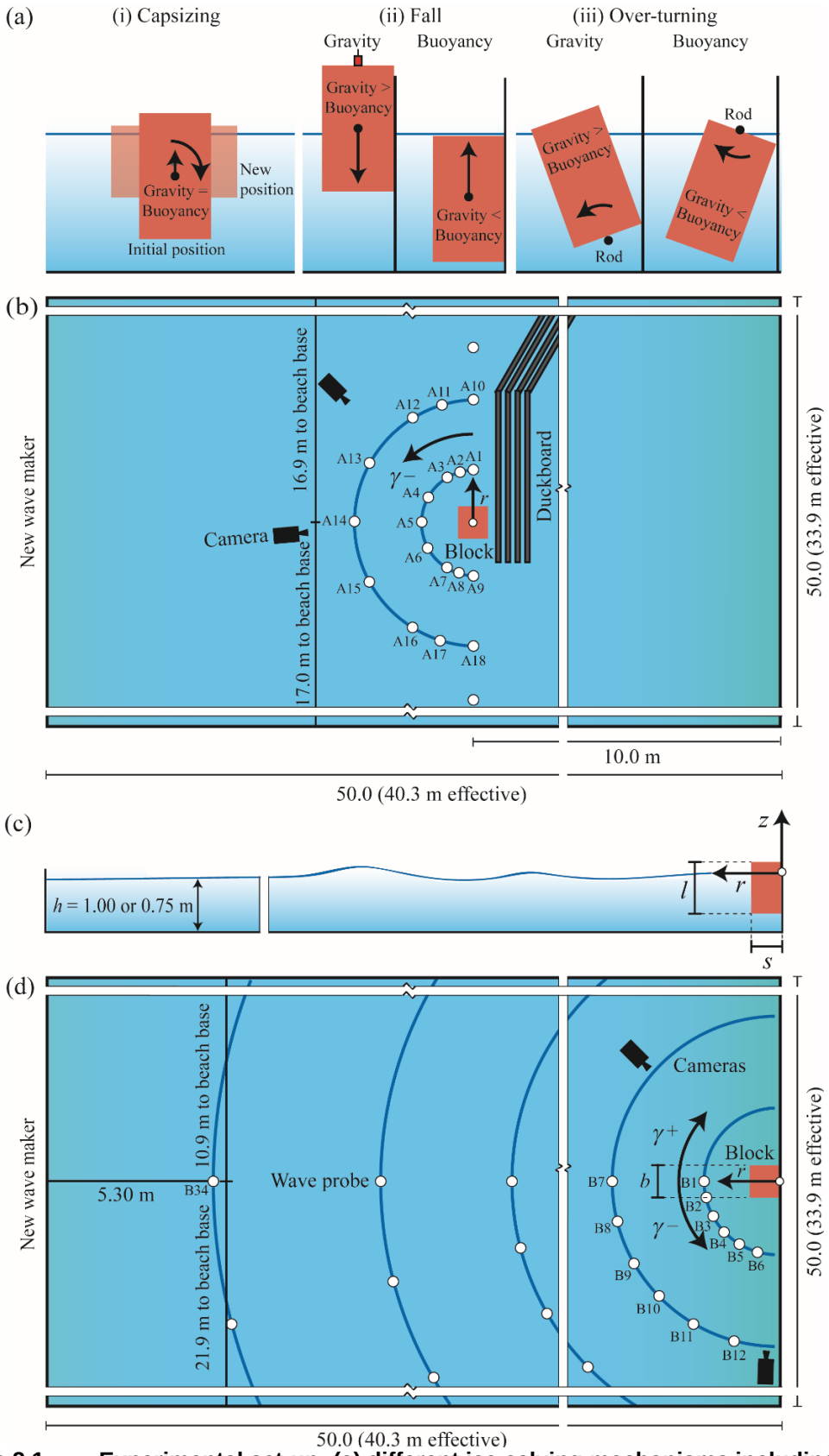


**Figure 2.1:** **Experimental set-up: (a) different ice calving mechanisms including (i) capsizing, (ii) fall (gravity and buoyancy dominated) and (iii) over-turning (gravity and buoyancy dominated), (b) plane view of capsizing case and (c,d) side and plane view of fall experiments. A selection of the numbered wave probes is given, with full details being available from Table 3.1 (not to scale).**

## 2.2 Definition of the coordinate system

The coordinate origins of the cylindrical coordinate systems ($r$, $z$, $\gamma$) are shown in Fig. 2.1b, c and d. The origins are located for all calving mechanisms in vertical direction $z$ on the water surface. In the horizontal plane the origin is located at the block centre for the capsizing case (Fig. 2.1b) and at the front of the steel plate in the centre of the block in cross-shore direction for all other calving mechanisms (Fig. 2.1c and d). The wave propagation angle $\gamma$ (angular angle) is defined positive in clockwise direction.

## 2.3 Relevant fixed parameters

Most dimensionless wave probe locations $r/h$ were held constant for all calving mechanisms to allow for cross-comparison of the tsunamigenic potential between the different ice calving mechanisms. The distance between the rod centre and block surface is 0.048 m for all over-turning cases (bottom right picture in Appendix A, Fig. 2.1aiii). The water temperature was 19.3°C ±0.4°C.

# 3 Instrumentation and data acquisition

## 3.1 Instruments

The block kinematics was recorded with a 9 Degree of Freedom (DoF) motion sensor (Adafruit BNO055, Fig. 3.1), two cameras (5 MP PointGrey ZBR2-PGEHD-50S5C-CS (used at 15 Hz) and 2 MP IOIndustries Flare 2M280-CXP (used at 100 Hz)) are used for general observations (Fig. 2.1b and d, Table 3.1) and the wave features were recorded in different directions with resistance type wave probes as shown in Fig. 2.1b and d as well as in Table 3.1. The wave probes are numbered anti-clockwise starting at $\gamma = 0°$ and from smaller to higher distance $r$ (Fig. 2.1b, d).

The motion sensor was located in a black enclosure which was screwed on the surface of the blocks as shown in Fig. 3.1. For all tests, the centre of the motion sensor was located 0.151 m on the left-hand side of the block centres. For the sphere tests it was located in the centre on top (fall gravity dominated) and bottom (fall buoyancy dominated) of the sphere. Table 4.2 shows the $x$- and $z$-locations of the sensor for all experiments, which were required to transform the measurements of the motion sensor from local to global coordinates and to extract the global positions and velocities. The values in the $z$-direction are evaluated from the position of the bottom of block or sphere relative to the water surface (given in the file name), the block or sphere length and the 3 mm distance of the motion sensor from the outside bottom of the enclosure.

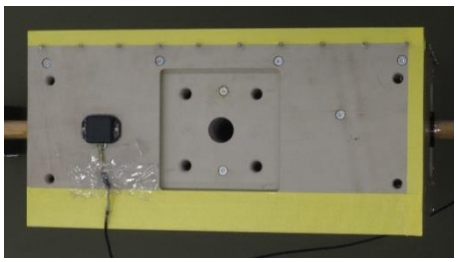

**Figure 3.1 Picture showing the location of the motion sensor in the black enclosure during a capsizing test of block 2**

**Table 3.1 Name and locations of wave probes and cameras**

| Ice calving mechanism | Device | Water depth $h$ (m) | Locations in function of the radial distance $r$ (m) and the wave propagation angle $\gamma$(°) (Fig. 2.1b and d) |
|---|---|---|---|
| Capsizing | Wave probes | 1.000 | A1 (2, 0); A10 (3, 0); A19 (5, 0); A28 (10, 0); A32 (15, 0);<br>A2 (2, –15); A11 (3, –15); A20 (5, –15); A29 (10, –15);<br>A3 (2, –30); A12 (3, –30); A21 (5, –30);<br>A4 (2, –60); A13 (3, –60); A22 (5, –60);<br>A5 (2, –90); A14 (3, –90); A23 (5, –90);<br>A6 (2, –120); A15 (3, –120); A24 (5, –120);<br>A7 (2, –150); A16 (3, –150); A25 (5, –150);<br>A8 (2, –165); A17 (3, –165); A26 (5, –165); A30 (10, –165);<br>A9 (2, –180); A18 (3, –180); A27 (5, –180); A31 (10, –180);<br>A33 (15, –180) |
| Capsizing | Cameras | 1.000 | 5 MP at 15 Hz: (6, –45); 2 MP at 100 Hz: (6, –95) |
| Fall/over-turning | Wave probes | 1.000 | B1 (2, 0); B7 (3, 0); B13 (5, 0); B19 (10, 0); B25 (15, 0); B31 (22.5, 0); B34 (35, 0);<br>B2 (2, –15); B8 (3, –15); B14 (5, –15); B20 (10, –15); B26 (15, –15); B32 (22.5, –15); B35 (35, –15);<br>B3 (2, –30); B9 (3, –30); B15 (5, –30); B21 (10, –30); B27 (15, –30); B33 (22.5, –30);<br>B4 (2, –45); B10 (3, –45); B16 (5, –45); B22 (10, –45); B28 (15, –45);<br>B5 (2, –60); B11 (3, –60); B17 (5, –60); B23 (10, –60); B29 (15, –60);<br>B6 (2, –75); B12 (3, –75); B18 (5, –75); B24 (10, –75); B30 (15, –75) |
| Fall/over-turning | Wave probes | 0.750 | C1 (1.5, 0); C7 (2.25, 0); C13 (3.75, 0); C19 (7.5, 0); C25 (11.25, 0); C31 (16.875, 0); C34 (26.25, 0);<br>C2 (1.5, –15); C8 (2.25, –15); C14 (3.75, –15); C20 (7.5, –15); C26 (11.25, –15); C32 (16.875, –15); C35 (26.25, –15);<br>C3 (1.5, –30); C9 (2.25, –30); C15 (3.75, –30); C21 (7.5, –30); C27 (11.25, –30); C33 (16.875, –30);<br>C4 (1.5, –45); C10 (2.25, –45); C16 (3.75, –45); C22 (7.5, –45); C28 (11.25, –45);<br>C5 (1.5, –60); C11 (2.25, –60); C17 (3.75, –60); C23 (7.5, –60); C29 (11.25, –60);<br>C6 (1.5, –75); C12 (2.25, –75); C18 (3.75, –75); C24 (7.5, –75); C30 (11.25, –75) |
| Fall/over-turning | Cameras | 1.000 and 0.750 | 2 MP at 100 Hz: (6, –85); 5 MP at 15 Hz: (6, 45) |

## 3.2 Definition of time origin and instrument synchronisation

The experiments included two independently triggered systems: system (a) included the wave probes, both cameras and a synchronisation pulse and system (b) included the motion sensor and the electromagnet (for the tests where it was in use). The motion sensor and the electromagnet were both recorded via a NI9205 module from National Instruments and a purpose-built program in LabView. The synchronisation pulse of (a) was recorded via the LabView programme and used to synchronise (a) and (b). Both the motion sensor and the high-speed camera were used to evaluate when the blocks started to move ($t$ = 0 s). Both methods agreed within 0.1 s for most tests, apart from some capsizing and over-turning (buoyancy dominated) tests where the mass moved very slowly (resulting in up to 1.2 s deviations between the two methods). The values evaluated from the high-speed camera were finally used to specify $t$ = 0 s, with exception of the tests where the block was initially submerged. The time in the wave probe and motion sensor "raw" files were shifted accordingly, before the main data analysis started. The motion sensor signals were sampled at full rate (at variable sampling rates with a mean of 74 Hz), the wave probes at 100 Hz and the cameras at 15 Hz (5 MP) and 100 Hz (2 MP), respectively. The wave gauge signals were filtered with a low-pass filter (Section 5).

## 3.3 Measured parameters

Prior to an experiment, when the block was put in place, the distance *z* of the block bottom from the still water surface was measured as well as the water temperature for some selected tests. During experiments the motion sensor attached to the blocks measured the block acceleration along the three local axes (*x*, *y*, *z*) (m), the three global angles (°) and the gravity field in three directions. Note that the sensor was not calibrated relative to the gravity field such that these data cannot be used. The water surface (m) was measured with 33 (capsizing) and 35 wave probes (all other ice calving mechanisms) and videos were recorded with two cameras at the locations given in Table 3.1.

# 4 Experimental procedure and test programme

The test programme included 73 experiments (62 individual tests plus 11 repetitions) as shown in Table 4.1 and the individual tests are in addition listed in Table 4.2. The capsizing mechanism involved 16 experiments, the fall mechanism 30 (21 gravity and 9 buoyancy dominated), the over-turning mechanism 20 (14 gravity and 6 buoyancy dominated) experiments and 7 fall experiments were conducted with a sphere (4 gravity and 3 buoyancy dominated). Each of the three calving mechanism (Fig. 2.1a) involved a different experimental procedure:

**Capsizing (case (i) in Fig. 2.1a and Fig. 5.1c):** The blocks in the capsizing case were hold in position with a wooden rod guided through the centre of the blocks (Fig. 5.1c). This rod was hold in position on both sides with steel profiles rigidly connected to a steel plate lying flat on the basin bottom, with the rod able to translate in vertical direction (but not sideward or forward) and rotate. The rotation of the block was initiated in most cases by removing a fitting which stabilised the block. For block 1 the block had to be slightly pushed by hand (with a force in the order of 1 N) to initiate capsizing. In some tests the blocks were pushed harder to investigate the effect of an increased rotation speed on the wave features.

**Fall (case (ii) in Fig. 2.1a, Fig. 5.1a,b and picture on title page):** The blocks were hold in position with an electromagnet prior to release, which was connected to a rope as shown in Fig. 2.1aii and the picture on the title page. The supporting frame for this electromagnet and the block was fixed to a steel plate at the basin wall. The blocks were moved in vertical direction with a winch system which was fixed to a support structure outside the wave basin. For the fall buoyancy case (right-hand side in Fig. 2.1aii), the block was pulled under water with a rope attached to the centre of the block bottom (Fig. 5.1) to support the buoyancy force of up to 200 N. For some buoyancy dominated tests the block had to be stabilised in addition with a steel beam from above and both the steel beam and the rope were then released simultaneously (similarly as the steel beam used for the over-turning buoyancy case shown in the bottom right picture in Appendix A). Note that experiments ts1 - ts7 were conducted with a basketball of diameter 0.215 m filled with water to achieve a density similar to ice. The drag force and terminal velocity of a sphere moving in fluid are well known as well as the radiated wave field of an oscillating sphere on the water surface. A comparison with analytical results may therefore be possible.

**Over-turning (case (iii) in Fig. 2.1a, Fig. 5.1a,b and bottom right picture in Appendix A):** The blocks were rotated around a fixed axis defined with a steel rod of 30 mm diameter. This rod was fed through two ball bearings fixed to the block surface (Fig. 5.2). This ensured that the blocks underwent a pure rotation, without any translation. The rod was hold in position with a UPN 80 steel profile on either side. The rod was located either below (left-hand side of case (iii) in Fig. 2.1a) or above the block (right-hand side of case (iii) in Fig. 2.1a). For some buoyancy dominated tests the block had to be stabilised in addition with a steel beam from above and the blocks started to move as soon as the steel beam was removed (bottom right picture in Appendix A).

**Table 4.1 Overview of all investigated test parameters of the 73 tests; Note that the block densities changed slightly depending on the attachments to the blocks (rod, clamp screws, plate to connect electromagnet, bearing); The number of runs indicated with + include test repetitions**

| Mass parameters | (i) Capsizing | | | (iii) Over-turning | | | |
|---|---|---|---|---|---|---|---|
| Mass release location | Offshore | Offshore | Offshore | At shore | At shore | At shore | At shore |
| Mass type | 1 | 2 | 2 | 1 | 2 | 2 | 2 |
| Mass length $l$ (m) | 0.800 | 0.800 | 0.500 | 0.800 | 0.800 | 0.500 | 0.500 |
| Mass width $b$ (m) | 0.500 | 0.500 | 0.800 | 0.500 | 0.500 | 0.800 | 0.800 |
| Mass thickness $s$ (m) | 0.500 | 0.250 | 0.250 | 0.500 | 0.250 | 0.250 | 0.250 |
| Mass volume $V_s$ ($m^3$) | 0.200 | 0.100 | 0.100 | 0.200 | 0.100 | 0.100 | 0.100 |
| Mass density $\rho_s$ ($kg/m^3$) | 929 | 924 | 924 | 936/923 | 912 | 912 | 936/912 |
| Mass $m_s$ (kg) | 185.8 | 92.4 | 92.3 | 187.1/184.6 | 91.2 | 91.2 | 93.6/91.2 |
| Water depth $h$ (m) | 1.000 | 1.000 | 1.000 | 1.000 | 1.000 | 1.000 | 0.750 |
| Release position above SWL (cm) (0 cm corresponds to SWL) | Neut. buoyant | Neut. buoyant | Neut. buoyant | 15, 0, -30, -60, -90 | 15, 0, -30, -60, -90 | 15, 0, -30, -60 | 15, 0, -30, -60 |
| No. of runs (73 in total) | $5^+$ | $6^+$ | $5^+$ | 5 | 5 | 4 | $6^+$ |

| Mass parameters | (ii) Fall | | | | | | |
|---|---|---|---|---|---|---|---|
| Mass release location | At shore | At shore | At shore | At shore | At shore | At shore | At shore |
| Mass type | 1 | 2 | 1 | 1 | 2 | 2 | sphere |
| Mass length $l$ (m) | 0.800 | 0.800 | 0.500 | 0.500 | 0.500 | 0.500 | 0.215 |
| Mass width $b$ (m) | 0.500 | 0.500 | 0.800 | 0.800 | 0.800 | 0.800 | 0.215 |
| Mass thickness $s$ (m) | 0.500 | 0.250 | 0.500 | 0.500 | 0.250 | 0.250 | 0.215 |
| Mass volume $V_s$ ($m^3$) | 0.200 | 0.100 | 0.200 | 0.200 | 0.100 | 0.100 | 0.005 |
| Mass density $\rho_s$ ($kg/m^3$) | 936/923 | 936/912 | 936/923 | 936/923 | 936/912 | 936/912 | 922 |
| Mass $m_s$ (kg) | 187.1/184.6 | 93.6/91.2 | 187.1/184.6 | 187.1/184.6 | 93.6/91.2 | 93.6/91.2 | 4.8 |
| Water depth $h$ (m) | 1.000 | 1.000 | 1.000 | 0.750 | 1.000 | 0.750 | 0.750 |
| Release position above SWL (cm) (0 cm corresponds to SWL) | 0, -30, -60, -84 | 0, -30, -60, -83 | 30, 0, -30, -60, -70, -83 | 30, 0, -30, -60 | 30, 0, -30, -60, -83 | 30, 0, -30, -60 | 54, 32, 11, 0, -11, -32, -43 |
| No. of runs (73 in total) | $6^+$ | 4 | $7^+$ | 4 | 5 | 4 | 7 |

**Table 4.2 Experimental parameters and dimensions of blocks in different ice calving mechanisms; all tests were run with either a block or a sphere; The file names include: Test ID_type of data (waves/motion)_calving mechanism (capsizing/fall_gravity/fall_buoyancy/over-turning_gravity/ over-turning_buoyancy)_block type (1/2/sphere)_water depth (100cm/ 75cm)_position of bottom of block or sphere relative to water surface (neutral/xcm); The position of the motion sensor is given in global coordinates with the origin on the water surface and *x* in *r* direction and *z* positive upwards; the *y* values for the motion sensor are 0.151 m for all tests except for the sphere where *y* = 0; *The total block masses changed slightly depending on the attachments to the blocks (rod, clamp screws, plate to connect electromagnet, bearing); **The motion sensor is located 3 mm above the outside bottom of the enclosure**

| Test ID | File name wave probes/motion sensor | Total mass * [kg] | Block length *l* [m] | Block width *b* [m] | Block thick-ness *s* [m] | *x* (m) position motion sensor | *z* (m) position motion sensor** | Comment |
|---|---|---|---|---|---|---|---|---|
| t1a | t1a_waves/motion_capsizing_ block2_100cm_-73.9cm | 92.43 | 0.800 | 0.500 | 0.250 | 0 | 0.061 + 0.003 = 0.064 | Block naturally over-turning; Coordinate origin in centre of block for all capsizing cases (Fig. 2.1b) |
| t1b | t1b_waves/motion_capsizing_ block2_100cm_-73.9cm | 92.43 | 0.800 | 0.500 | 0.250 | 0 | 0.064 | Repetition |
| t1c | t1c_waves/motion_capsizing_ block2_100cm_-73.9cm | 92.43 | 0.800 | 0.500 | 0.250 | 0 | 0.064 | Repetition |
| t2 | t2_waves/motion_capsizing_ block2_100cm_-73.9cm | 92.43 | 0.800 | 0.500 | 0.250 | 0 | 0.064 | Block pushed |
| t3 | t3_waves/motion_capsizing_ block2_100cm_-73.9cm | 92.43 | 0.800 | 0.500 | 0.250 | 0 | 0.064 | Block pushed |
| t4 | t4_waves/motion_capsizing_ block2_100cm_-73.9cm | 92.43 | 0.800 | 0.500 | 0.250 | 0 | 0.064 | Block pushed |

| | | | | | | | | |
|---|---|---|---|---|---|---|---|---|
| t5a | t5a_waves/motion_capsizing_block2_100cm_-46.2cm | 92.26 | 0.500 | 0.800 | 0.250 | 0 | 0.038 + 0.003 = 0.041 | Block naturally over-turning |
| t5b | t5b_waves/motion_capsizing_block2_100cm_-46.2cm | 92.26 | 0.500 | 0.800 | 0.250 | 0 | 0.041 | Repetition |
| t5c | t5c_waves/motion_capsizing_block2_100cm_-46.2cm | 92.26 | 0.500 | 0.800 | 0.250 | 0 | 0.041 | Repetition |
| t6 | t6_waves/motion_capsizing_block2_100cm_-46.2cm | 92.26 | 0.500 | 0.800 | 0.250 | 0 | 0.041 | Block pushed |
| t7 | t7_waves/motion_capsizing_block2_100cm_-46.2cm | 92.26 | 0.500 | 0.800 | 0.250 | 0 | 0.041 | Block pushed |
| t8a | t8a_waves/motion_capsizing_block1_100cm_-74.3cm | 185.75 | 0.800 | 0.500 | 0.500 | 0 | 0.057 + 0.003 = 0.060 | Block stable (slightly pushed) |
| t8b | t8b_waves/motion_capsizing_block1_100cm_-74.3cm | 185.75 | 0.800 | 0.500 | 0.500 | 0 | 0.060 | Repetition |
| t8c | t8c_waves/motion_capsizing_block1_100cm_-74.3cm | 185.75 | 0.800 | 0.500 | 0.500 | 0 | 0.060 | Repetition |
| t9 | t9_waves/motion_capsizing_block1_100cm_-74.3cm | 185.75 | 0.800 | 0.500 | 0.500 | 0 | 0.060 | Block more pushed |
| t10 | t10_waves/motion_capsizing_block1_100cm_-74.3cm | 185.75 | 0.800 | 0.500 | 0.500 | 0 | 0.060 | Block more pushed |
| t11 | t11_waves/motion_fall_gravity_block2_100cm_-60cm | 93.62 | 0.800 | 0.500 | 0.250 | 0.125 | 0.800 – 0.600 + 0.003 = 0.203 | For the remaining tests the coordinate origin is at the wall (Fig. 2.1c,d) |
| t12 | t12_waves/motion_fall_gravity_block2_100cm_-30cm | 93.62 | 0.800 | 0.500 | 0.250 | 0.125 | 0.503 | |
| t13 | t13_waves/motion_fall_gravity_block2_100cm_0cm | 93.62 | 0.800 | 0.500 | 0.250 | 0.125 | 0.803 | |
| t14 | t14_waves/motion_fall_gravity_block2_100cm_-30cm | 93.62 | 0.500 | 0.800 | 0.250 | 0.125 | 0.203 | |
| t15 | t15_waves/motion_fall_gravity_block2_100cm_0cm | 93.62 | 0.500 | 0.800 | 0.250 | 0.125 | 0.503 | |
| t16 | t16_waves/motion_fall_gravity_block2_100cm_30cm | 93.62 | 0.500 | 0.800 | 0.250 | 0.125 | 0.803 | |
| t17 | t17_waves/motion_fall_gravity_block1_100cm_-60cm | 187.11 | 0.800 | 0.500 | 0.500 | 0.250 | 0.203 | |
| t18 | t18_waves/motion_fall_gravity_block1_100cm_-30cm | 187.11 | 0.800 | 0.500 | 0.500 | 0.250 | 0.503 | |
| t19a | t19a_waves/motion_fall_gravity_block1_100cm_0cm | 187.11 | 0.800 | 0.500 | 0.500 | 0.250 | 0.803 | |
| t19b | t19b_waves/motion_fall_gravity_block1_100cm_0cm | 187.11 | 0.800 | 0.500 | 0.500 | 0.250 | 0.803 | Repetition |
| t19c | t19c_waves/motion_fall_gravity_block1_100cm_0cm | 187.11 | 0.800 | 0.500 | 0.500 | 0.250 | 0.803 | Repetition |
| t20 | t20_waves/motion_fall_gravity_block1_100cm_-30cm | 187.11 | 0.500 | 0.800 | 0.500 | 0.250 | 0.203 | |
| t21 | t21_waves/motion_fall_gravity_block1_100cm_0cm | 187.11 | 0.500 | 0.800 | 0.500 | 0.250 | 0.503 | |
| t22a | t22a_waves/motion_fall_gravity_block1_100cm_30cm | 187.11 | 0.500 | 0.800 | 0.500 | 0.250 | 0.803 | |
| t22b | t22b_waves/motion_fall_gravity_block1_100cm_30cm | 187.11 | 0.500 | 0.800 | 0.500 | 0.250 | 0.803 | Repetition |
| t23 | t23_waves/motion_overturning_gravity_block1_100cm_0cm | 187.11 | 0.800 | 0.500 | 0.500 | 0.250 | 0.803 | Distance sensor from axis of rotation in *z*-direction = 0.803 + 0.048 (distance axis to block surface) = 0.851 m |
| t24 | t24_waves/motion_overturning_gravity_block1_100cm_-30cm | 187.11 | 0.800 | 0.500 | 0.500 | 0.250 | 0.503 | Distance sensor from axis of rotation in *z*-direction = 0.851 m |
| t25 | t25_waves/motion_overturning_gravity_block1_100cm_15cm | 187.11 | 0.800 | 0.500 | 0.500 | 0.250 | 0.953 | Distance sensor from axis of rotation in *z*-direction = 0.851 m |
| t26 | t26_waves/motion_overturning_gravity_block1_100cm_-60cm | 187.11 | 0.800 | 0.500 | 0.500 | 0.250 | 0.203 | Distance sensor from axis of rotation in *z*-direction = 0.851 m |

| | | | | | | | | |
|---|---|---|---|---|---|---|---|---|
| t27 | t27_waves/motion_overturning_gravity_block2_100cm_0cm | 91.15 | 0.800 | 0.500 | 0.250 | 0.125 | 0.803 | Distance sensor from axis of rotation in *z*-direction = 0.851 m |
| t28 | t28_waves/motion_overturning_gravity_block2_100cm_-30cm | 91.15 | 0.800 | 0.500 | 0.250 | 0.125 | 0.503 | Distance sensor from axis of rotation in *z*-direction = 0.851 m |
| t29 | t29_waves/motion_overturning_gravity_block2_100cm_-60cm | 91.15 | 0.800 | 0.500 | 0.250 | 0.125 | 0.203 | Distance sensor from axis of rotation in *z*-direction = 0.851 m |
| t30 | t30_waves/motion_overturning_gravity_block2_100cm_15cm | 91.15 | 0.800 | 0.500 | 0.250 | 0.125 | 0.953 | Distance sensor from axis of rotation in *z*-direction = 0.851 m |
| t31 | t31_waves/motion_overturning_gravity_block2_100cm_15cm | 91.15 | 0.500 | 0.800 | 0.250 | 0.125 | 0.653 | Distance sensor from axis of rotation in *z*-direction = 0.551 m |
| t32 | t32_waves/motion_overturning_gravity_block2_100cm_0cm | 91.15 | 0.500 | 0.800 | 0.250 | 0.125 | 0.503 | Distance sensor from axis of rotation in *z*-direction = 0.551 m |
| t33 | t33_waves/motion_overturning_gravity_block2_100cm_-30cm | 91.15 | 0.500 | 0.800 | 0.250 | 0.125 | 0.203 | Distance sensor from axis of rotation in *z*-direction = 0.551 m |
| t34 | t34_waves/motion_overturning_buoyancy_block2_100cm_-60cm | 91.15 | 0.500 | 0.800 | 0.250 | 0.125 | -0.600 – 0.003 = -0.603 | Distance sensor from axis of rotation in *z*-direction = 0.551 m |
| t35 | t35_waves/motion_overturning_buoyancy_block2_100cm_-90cm | 91.15 | 0.800 | 0.500 | 0.250 | 0.125 | -0.903 | Distance sensor from axis of rotation in *z*-direction = 0.851 m |
| t36 | t36_waves/motion_overturning_buoyancy_block1_100cm_-90cm | 184.64 | 0.800 | 0.500 | 0.500 | 0.250 | -0.903 | Distance sensor from axis of rotation in *z*-direction = 0.851 m |
| t37 | t37_waves/motion_fall_buoyancy_block1_100cm_-83.5cm | 184.64 | 0.800 | 0.500 | 0.500 | 0.250 | -0.835 + 0.800 – 0.003 = -0.032 | |
| t38 | t38_waves/motion_fall_buoyancy_block1_100cm_-60cm | 184.64 | 0.500 | 0.800 | 0.500 | 0.250 | -0.097 | |
| t39 | t39_waves/motion_fall_buoyancy_block1_100cm_-83cm | 184.64 | 0.500 | 0.800 | 0.500 | 0.250 | -0.327 | |
| t40 | t40_waves/motion_fall_buoyancy_block1_100cm_-70cm | 184.64 | 0.500 | 0.800 | 0.500 | 0.250 | -0.197 | |
| t41 | t41_waves/motion_fall_buoyancy_block2_100cm_-83cm | 91.15 | 0.800 | 0.500 | 0.250 | 0.125 | -0.027 | |
| t42 | t42_waves/motion_fall_buoyancy_block2_100cm_-60cm | 91.15 | 0.500 | 0.800 | 0.250 | 0.125 | -0.097 | |
| t43 | t43_waves/motion_fall_buoyancy_block2_100cm_-83cm | 91.15 | 0.500 | 0.800 | 0.250 | 0.125 | -0.327 | |
| t44 | t44_waves/motion_fall_gravity_block2_75cm_-30cm | 93.62 | 0.500 | 0.800 | 0.250 | 0.125 | 0.203 | |
| t45 | t45_waves/motion_fall_gravity_block2_75cm_0cm | 93.62 | 0.500 | 0.800 | 0.250 | 0.125 | 0.503 | |
| t46 | t46_waves/motion_fall_gravity_block2_75cm_30cm | 93.62 | 0.500 | 0.800 | 0.250 | 0.125 | 0.803 | |
| t47 | t47_waves/motion_fall_gravity_block1_75cm_30cm | 187.11 | 0.500 | 0.800 | 0.500 | 0.250 | 0.803 | |
| t48 | t48_waves/motion_fall_gravity_block1_75cm_0cm | 187.11 | 0.500 | 0.800 | 0.500 | 0.250 | 0.503 | |
| t49 | t49_waves/motion_fall_gravity_block1_75cm_-30cm | 187.11 | 0.500 | 0.800 | 0.500 | 0.250 | 0.203 | |
| t50 | t50_waves/motion_overturning_gravity_block2_75cm_15cm | 93.62 | 0.500 | 0.800 | 0.250 | 0.125 | 0.653 | Distance sensor from axis of rotation in *z*-direction = 0.551 m |
| t51 | t51_waves/motion_overturning_gravity_block2_75cm_0cm | 93.62 | 0.500 | 0.800 | 0.250 | 0.125 | 0.503 | Distance sensor from axis of ro- |

| | | | | | | | | |
|---|---|---|---|---|---|---|---|---|
| | | | | | | | | tation in *z*-direction = 0.551 m |
| t52 | t52_waves/motion_overturning_gravity_block2_75cm_-30cm | 93.62 | 0.500 | 0.800 | 0.250 | 0.125 | 0.203 | Distance sensor from axis of rotation in *z*-direction = 0.551 m |
| t53a | t53a_waves/motion_overturning_buoyancy_block2_75cm_-60cm | 91.15 | 0.500 | 0.800 | 0.250 | 0.125 | -0.603 | Distance sensor from axis of rotation in *z*-direction = 0.551 m |
| t53b | t53b_waves/motion_overturning_buoyancy_block2_75cm_-60cm | 91.15 | 0.500 | 0.800 | 0.250 | 0.125 | -0.603 | Repetition; Distance sensor from axis of rotation in *z*-direction = 0.551 m |
| t53c | t53c_waves/motion_overturning_buoyancy_block2_75cm_-60cm | 91.15 | 0.500 | 0.800 | 0.250 | 0.125 | -0.603 | Repetition; Distance sensor from axis of rotation in *z*-direction = 0.551 m |
| t54 | t54_waves/motion_fall_buoyancy_block2_75cm_-60cm | 91.15 | 0.500 | 0.800 | 0.250 | 0.125 | -0.097 | |
| t55 | t55_waves/motion_fall_buoyancy_block1_75cm_-60cm | 184.64 | 0.500 | 0.800 | 0.500 | 0.250 | -0.097 | |
| ts1 | ts1_waves/motion_fall_gravity_sphere_75cm_10.8cm | 4.80 | 0.215 | 0.215 | 0.215 | 0.108 | 0.108 + 0.215 + 0.003 = 0.326 | Test with sphere with sensor on top |
| ts2 | ts2_waves/motion_fall_gravity_sphere_75cm_32.2cm | 4.80 | 0.215 | 0.215 | 0.215 | 0.108 | 0.540 | Test with sphere with sensor on top |
| ts3 | ts3_waves/motion_fall_gravity_sphere_75cm_53.8cm | 4.80 | 0.215 | 0.215 | 0.215 | 0.108 | 0.756 | Test with sphere with sensor on top |
| ts4 | ts4_waves/motion_fall_gravity_sphere_75cm_0cm | 4.80 | 0.215 | 0.215 | 0.215 | 0.108 | 0.111 | Test with sphere with sensor on top |
| ts5 | ts5_waves/motion_fall_buoyancy_sphere_75cm_-10.8cm | 4.80 | 0.215 | 0.215 | 0.215 | 0.108 | -0.108 – 0.215 – 0.003 = -0.326 | Test with sphere with sensor on bottom |
| ts6 | ts6_waves/motion_fall_buoyancy_sphere_75cm_-32.2cm | 4.80 | 0.215 | 0.215 | 0.215 | 0.108 | -0.540 | Test with sphere with sensor on bottom |
| ts7 | ts7_waves/motion_fall_buoyancy_sphere_75cm_-42.5cm | 4.80 | 0.215 | 0.215 | 0.215 | 0.108 | -0.643 | Test with sphere with sensor on bottom |

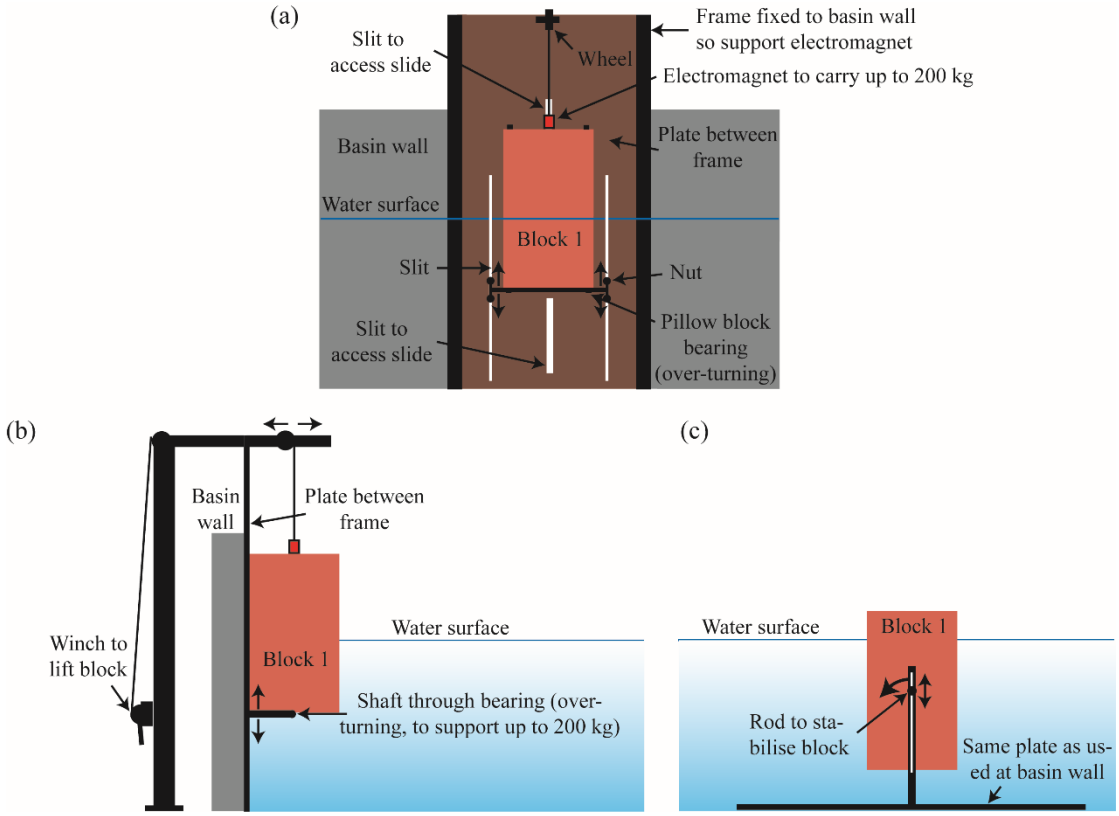


**Figure 5.1** **Design of experimental set-up: (a) front view and (b) side view of fall experiment (overlapped with some components for the over-turning case) and (c) side view of capsizing experiment (not to scale).**

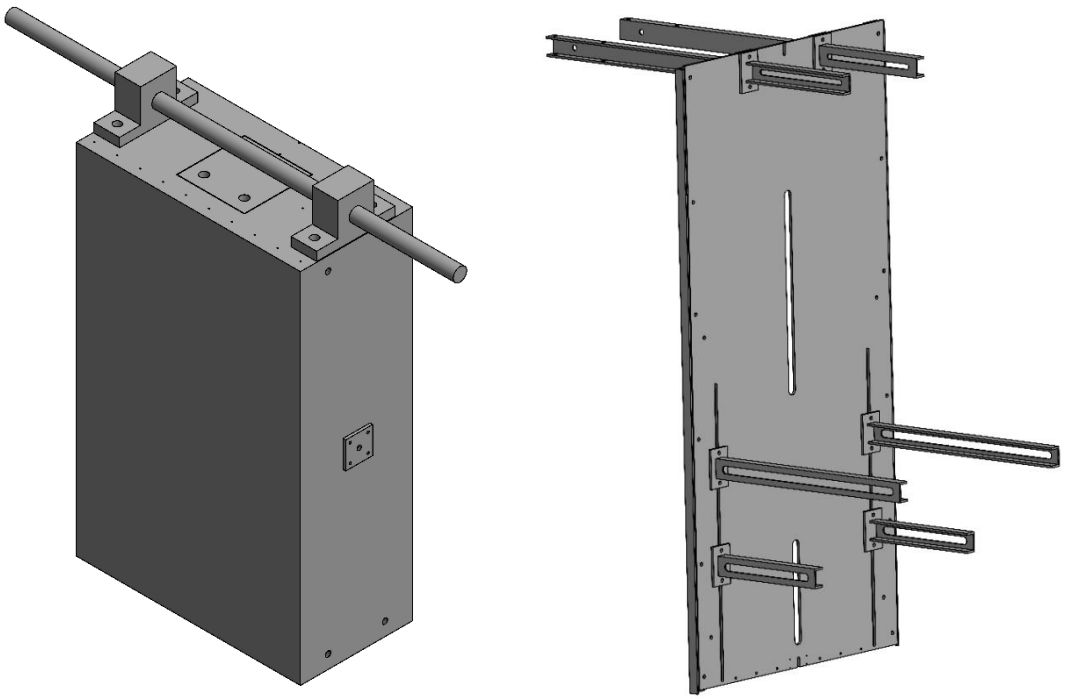

**Figure 5.2** **Technical drawings: (left) block 2 equipped with rod used for over-turning mechanism (Fig. 2.1aiii) and (right) steel plate including all steel profiles to hold the blocks in place; the plate was either lying flat on the basin bottom for the capsizing case (with all but the two long UPN profiles on the right-hand side removed) or fixed to the basin wall for all other cases (where the six remaining UPN profiles were used, for details see Appendix B).**

# 5 Data post-processing

The time columns of the wave probes and motion sensor files were adjusted such that $t$ = 0 s corresponds to the moment in time when the blocks or sphere started to move for experiments where they were initially in contact with the surrounding water, or at the moment in time when the blocks or sphere touched the water surface when they were initially not in contact with the water body. Unnecessary columns were removed (voltage signal from the electromagnet, uncalibrated data from motion sensor, etc.). The raw data of the motion sensor were further analysed in Matlab to transform the accelerations in global coordinates and to derive the block velocities and positions. The file name was then changed with the notation given in Table 4.2. These files are named “raw” ahead of the ending given in Table 4.2. The wave probe time series were shortened to remove reflections from the basin boundaries for all raw data. The wave probe data were then filtered with a low-pass filter with a cut off frequency at 9 to 11 Hz. For wave probes 9, 17 and 25 in the capzising experiments and 21, 24 and 32 for all fall and overturning experiments a low-pass filter with a cut off frequency at 3.0 or 3.5 Hz was applied to remove large high-frequency noise. For wave probes C30 and C31 in the experiments t53b, s5, s6, for wave probe C30 in s7 and for wave probe B32 in t41, the wave probe signals remained noisy after filtering given that the waves were extremely small, such that they were excluded from further analysis. The post processed data were then saved under the new name “post_processed_...”. ahead of the ending given in Table 4.2 and used for further analysis.

# 6 Organization of data files

The sets of data are given in text format; one file for each experiment contains the wave probe data (raw and post-processed) and one the motion sensor data. These three files are organised as follows:

*Motion sensor files (text file, no separator):*
Column 1: time (s) with $t$ = 0 s at the moment in time when the blocks started to move or touched the water surface
Column 2: global angle (°) relative to $x$-axis (pitch)
Column 3: global angle (°) relative to $y$-axis (roll)
Column 4: global angle (°) relative to $z$-axis (yaw)
Column 5: local acceleration (m/s$^2$) in $x$-direction
Column 6: local acceleration (m/s$^2$) in $y$-direction
Column 7: local acceleration (m/s$^2$) in $z$-direction

*Wave probe files (raw and post-processed, text data, no separator):*
Column 1: time (s) with $t$ = 0 s at the moment in time when the blocks started to move or touched the water surface
Column 2-34 (capsizing tests) and 2-36 (all other tests): water surface displacement (m)

*Organisation of the files on Zenodo:*
- DataStorageReport_Heller_Ice_Tsunamis.pdf
- Pictures_overview
- Videos
- Motion_sensor_data
- Wave_probe_data_raw
- Wave_probe_data_post_processed
- README

# 7 Publications

Chen, F., Heller, V. and Briganti, R. (2019). Numerical modelling of tsunamis generated by iceberg calving validated with large-scale laboratory experiments (in preparation).

Heller, V., Chen, F., Brühl, M., Gabl, R., Chen, X., Wolters, G. and Fuchs, H. (2019). Large-scale experiments into the tsunamigenic potential of different iceberg calving mechanisms. *Scientific Reports* 9:861 (www.nature.com/articles/s41598-018-36634-3).

# A Appendix: Pictures

Some pictures are shown below including the set-up of the capsizing case with block 1 (top), the steel structure at the basin wall including block 2 hold with the electromagnet (bottom left) and block 2 in the initial position for the over-turning buoyancy dominated mechanism with the steel rod as the axis of rotation.

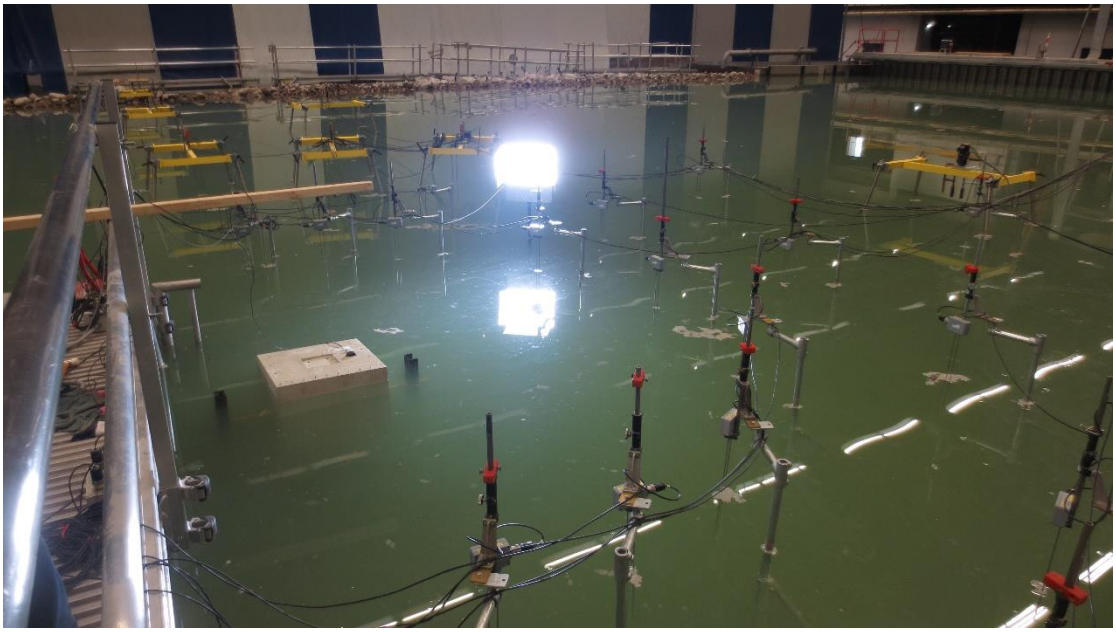

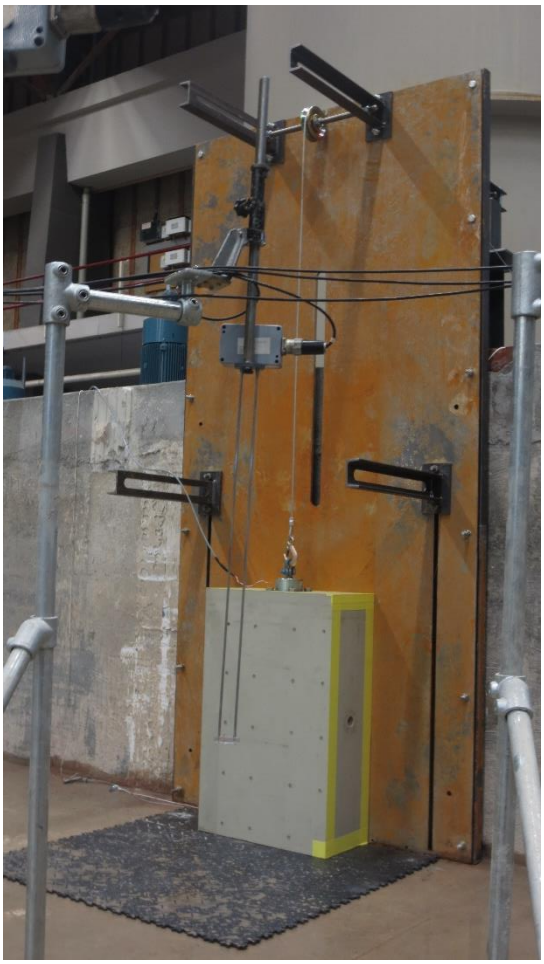

# B Appendix: Detailed technical drawings

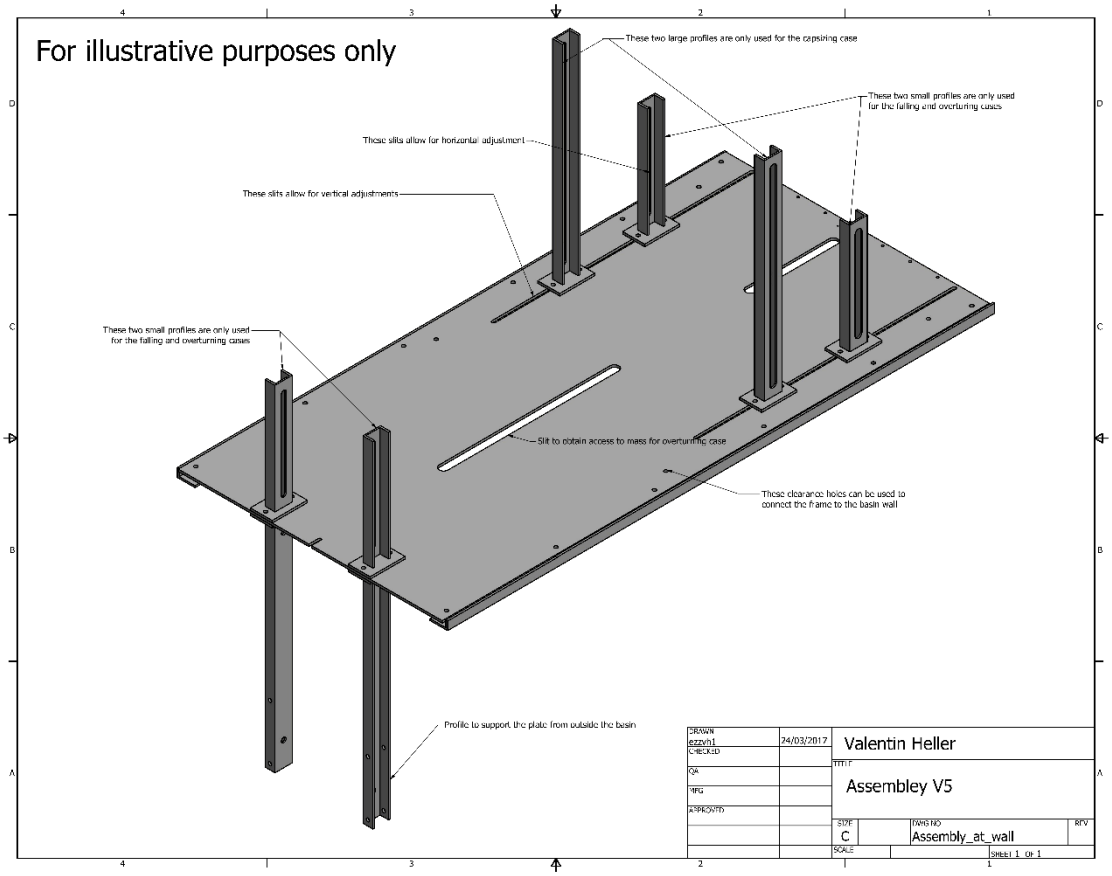


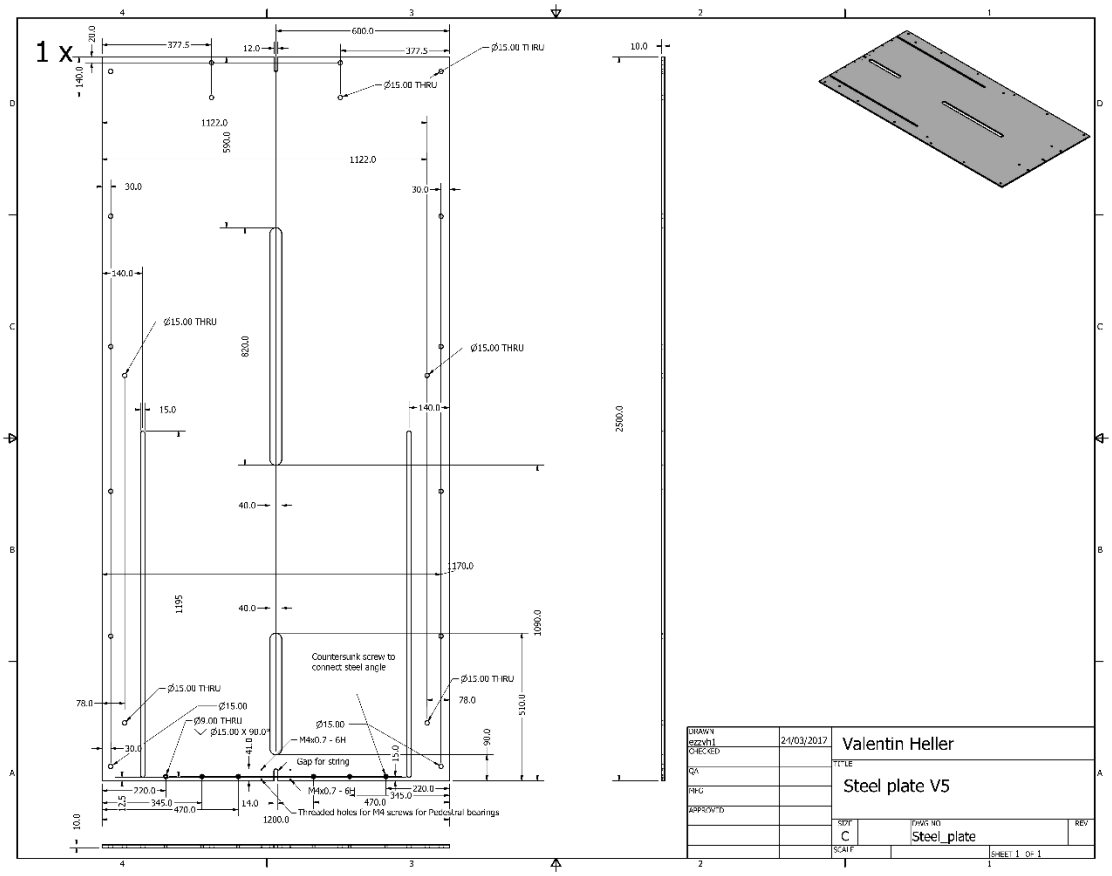

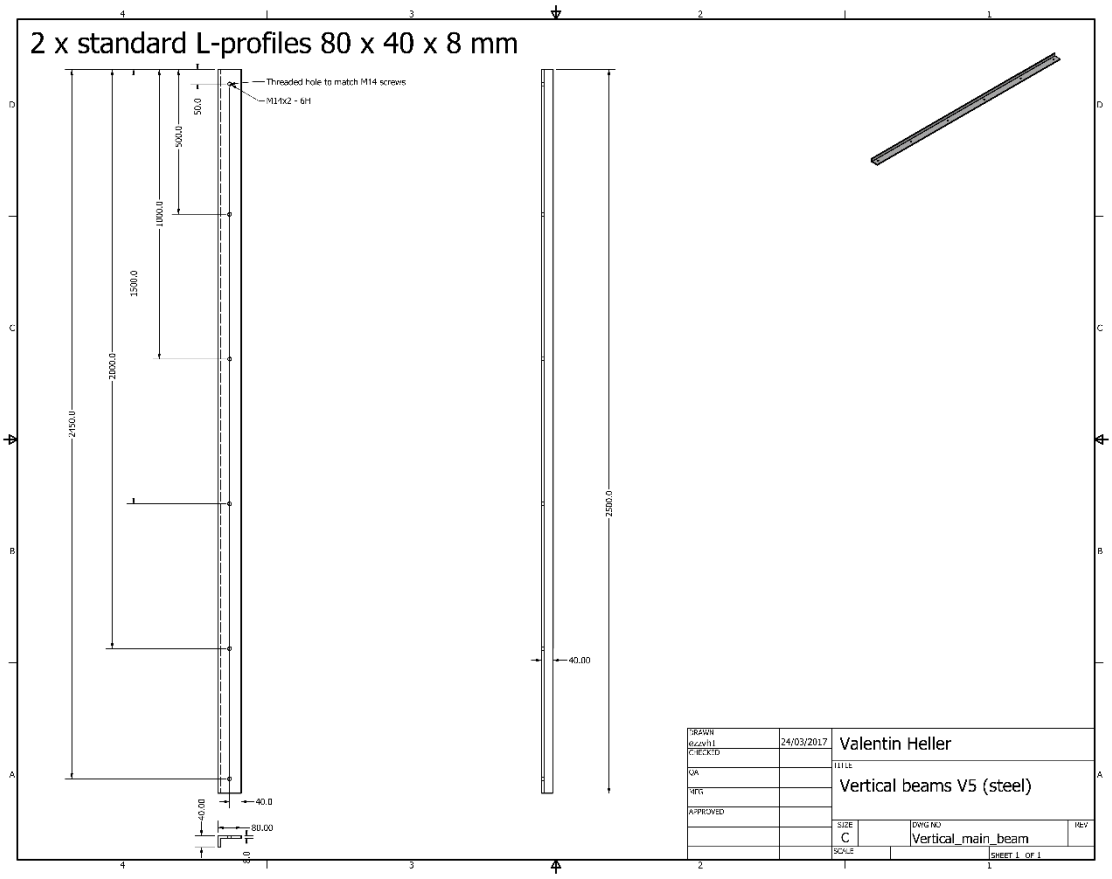
2 x standard L-profiles 80 x 40 x 8 mm
Threaded hole to match M14 screws
M14x2 - 6H
50.0
500.0
1000.0
1500.0
2000.0
2150.0
2500.0
40.00
40.0
40.00
80.00
8.0
DRAWN
ezzvh1
CHECKED
QA
MFG
APPROVED
24/03/2017
Valentin Heller
TITLE
Vertical beams V5 (steel)
SIZE
C
DWG NO
Vertical_main_beam
REV
SCALE
SHEET 1 OF 1

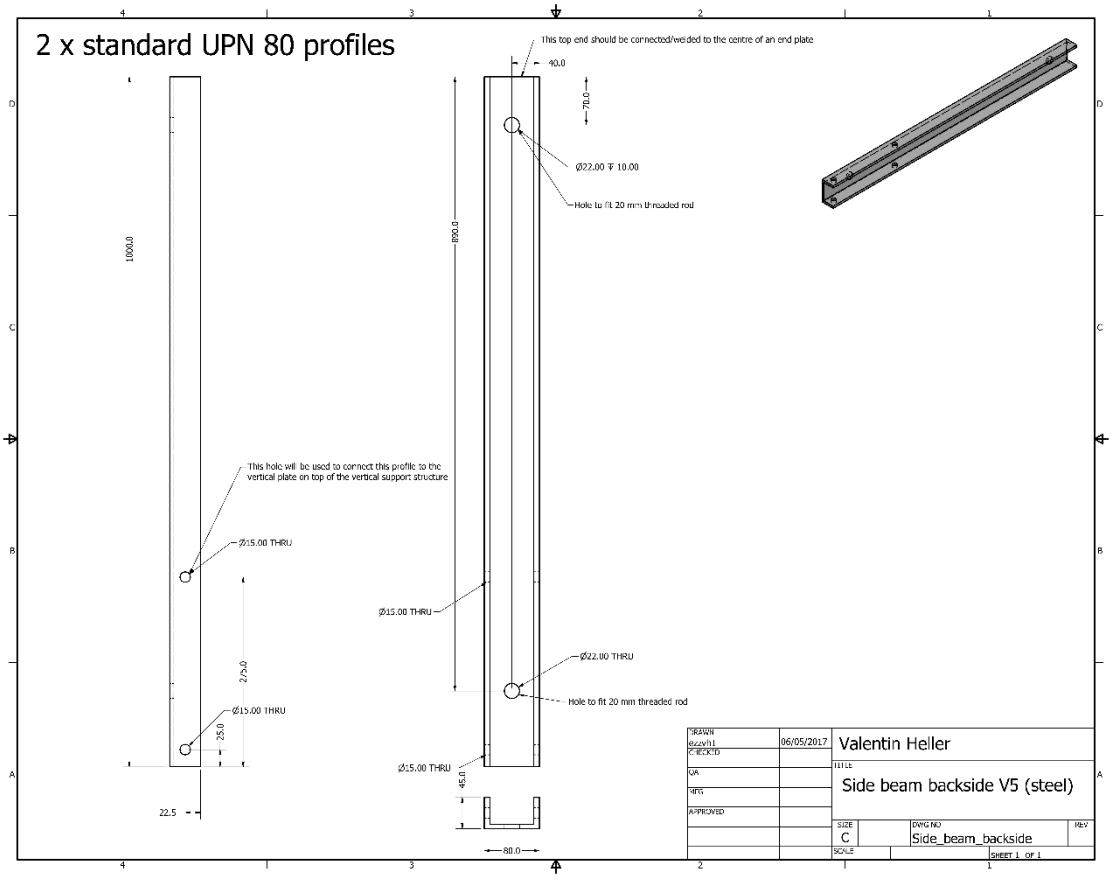
2 x standard UPN 80 profiles
This top end should be connected/welded to the centre of an end plate
40.0
70.0
Ø22.00 ₸ 10.00
Hole to fit 20 mm threaded rod
890.0
1000.0
This hole will be used to connect this profile to the vertical plate on top of the vertical support structure
Ø15.00 THRU
Ø15.00 THRU
Ø22.00 THRU
Hole to fit 20 mm threaded rod
Ø15.00 THRU
275.0
Ø15.00 THRU
25.0
22.5
45.0
80.0
DRAWN
ezzvh1
CHECKED
QA
MFG
APPROVED
06/05/2017
Valentin Heller
TITLE
Side beam backside V5 (steel)
SIZE
C
DWG NO
Side_beam_backside
REV
SCALE
SHEET 1 OF 1

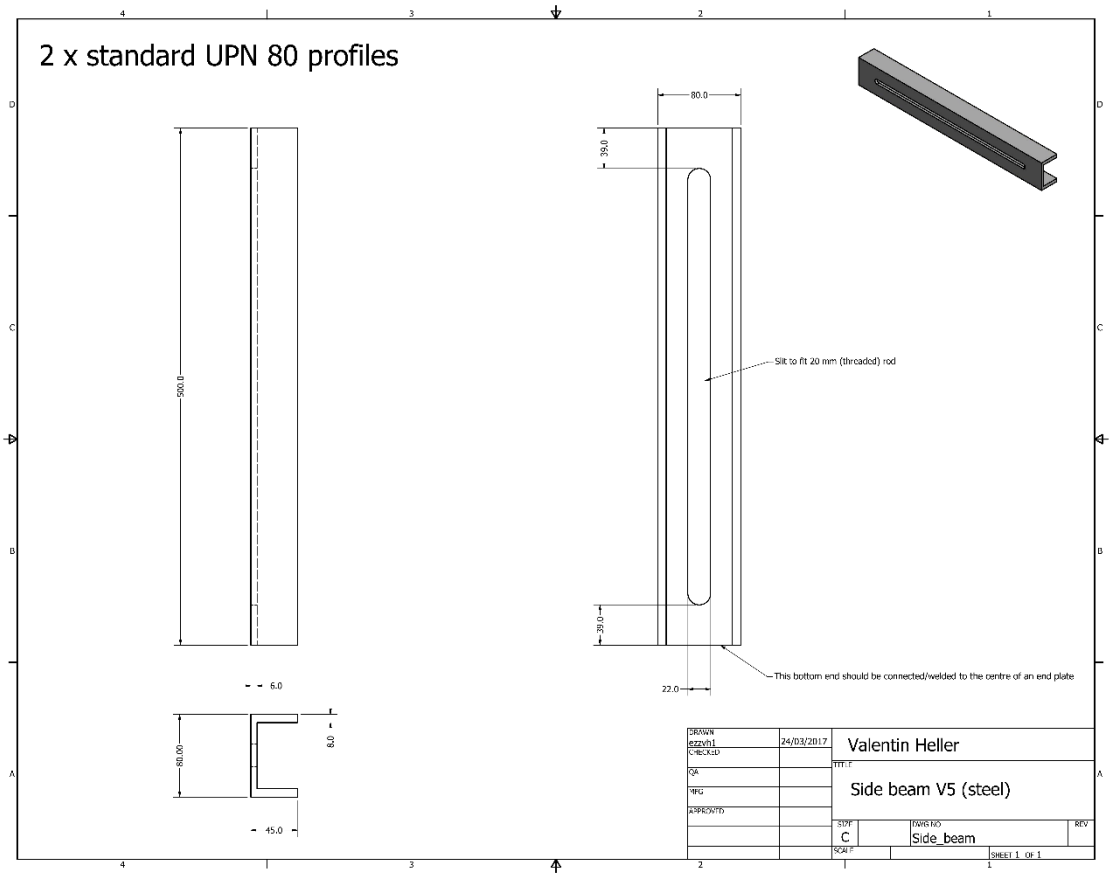
2 x standard UPN 80 profiles
80.0
35.0
500.0
Slit to fit 20 mm (threaded) rod
39.0
22.0
This bottom end should be connected/welded to the centre of an end plate
6.0
8.0
80.00
45.0
DRAWN
ezzvh1
24/03/2017
Valentin Heller
CHECKED
QA
MFG
APPROVED
TITLE
Side beam V5 (steel)
SIZE
C
DWG NO
Side_beam
REV
SCALE
SHEET 1 OF 1

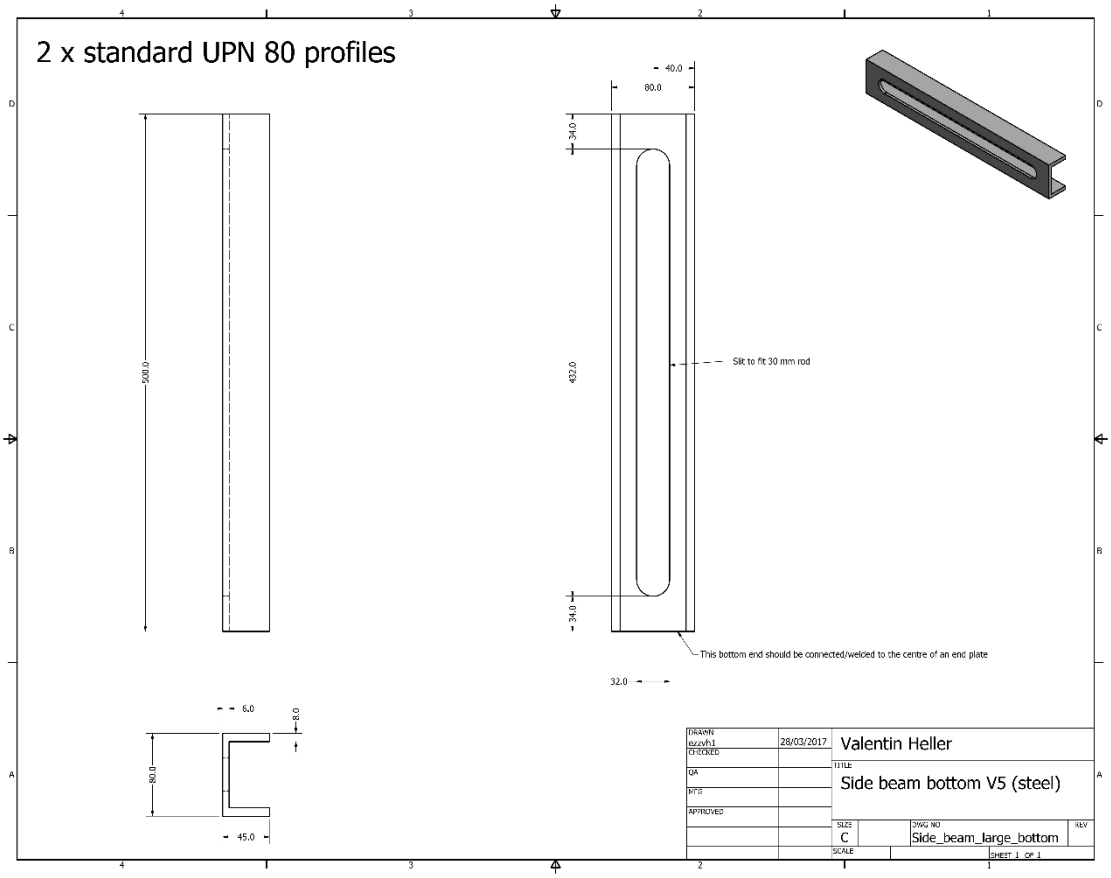
2 x standard UPN 80 profiles
40.0
80.0
34.0
500.0
Slit to fit 30 mm rod
432.0
34.0
This bottom end should be connected/welded to the centre of an end plate
32.0
6.0
8.0
80.0
45.0
DRAWN
ezzvh1
28/03/2017
Valentin Heller
CHECKED
QA
MFG
APPROVED
TITLE
Side beam bottom V5 (steel)
SIZE
C
DWG NO
Side_beam_large_bottom
REV
SCALE
SHEET 1 OF 1

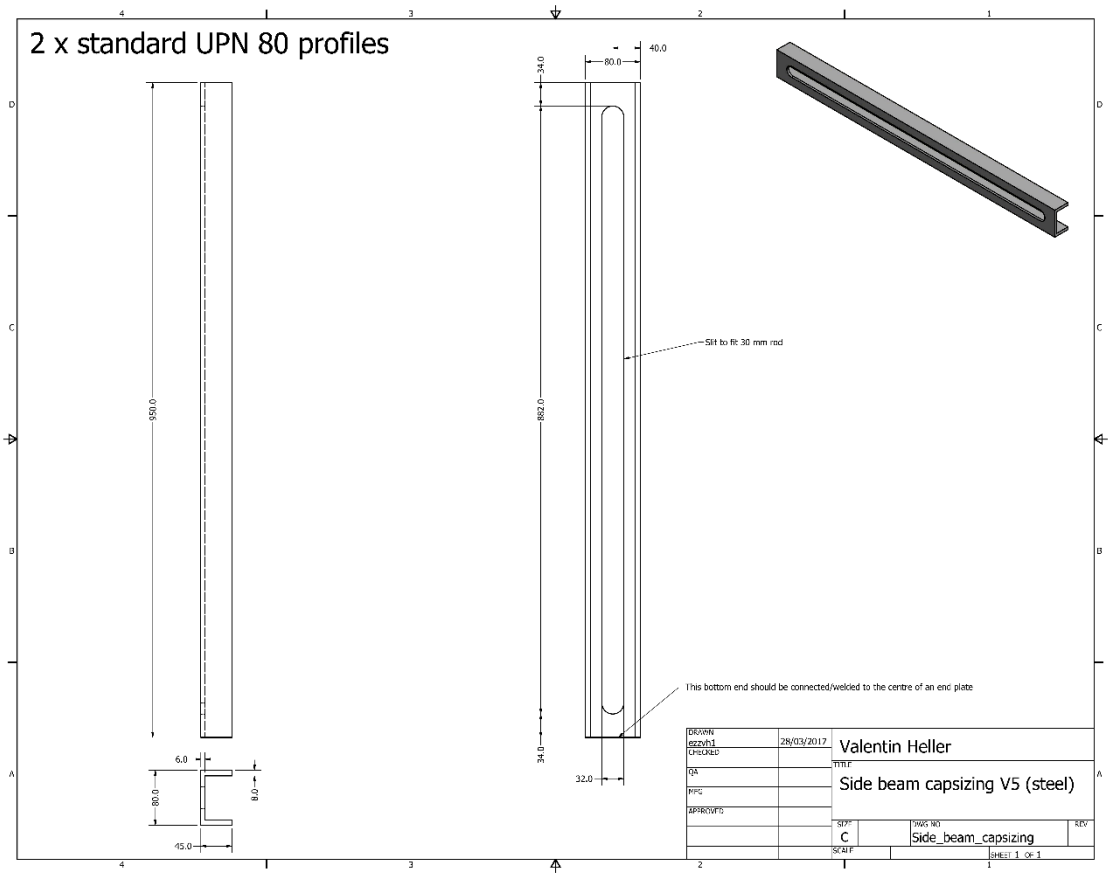
2 x standard UPN 80 profiles
40.0
80.0
34.0
950.0
882.0
Slit to fit 30 mm rod
This bottom end should be connected/welded to the centre of an end plate
34.0
32.0
6.0
80.0
8.0
45.0
DRAWN
ezzvh1
28/03/2017
Valentin Heller
CHECKED
QA
MFG
APPROVED
TITLE
Side beam capsizing V5 (steel)
SIZE
C
DWG NO
Side_beam_capsizing
REV
SCALE
SHEET 1 OF 1

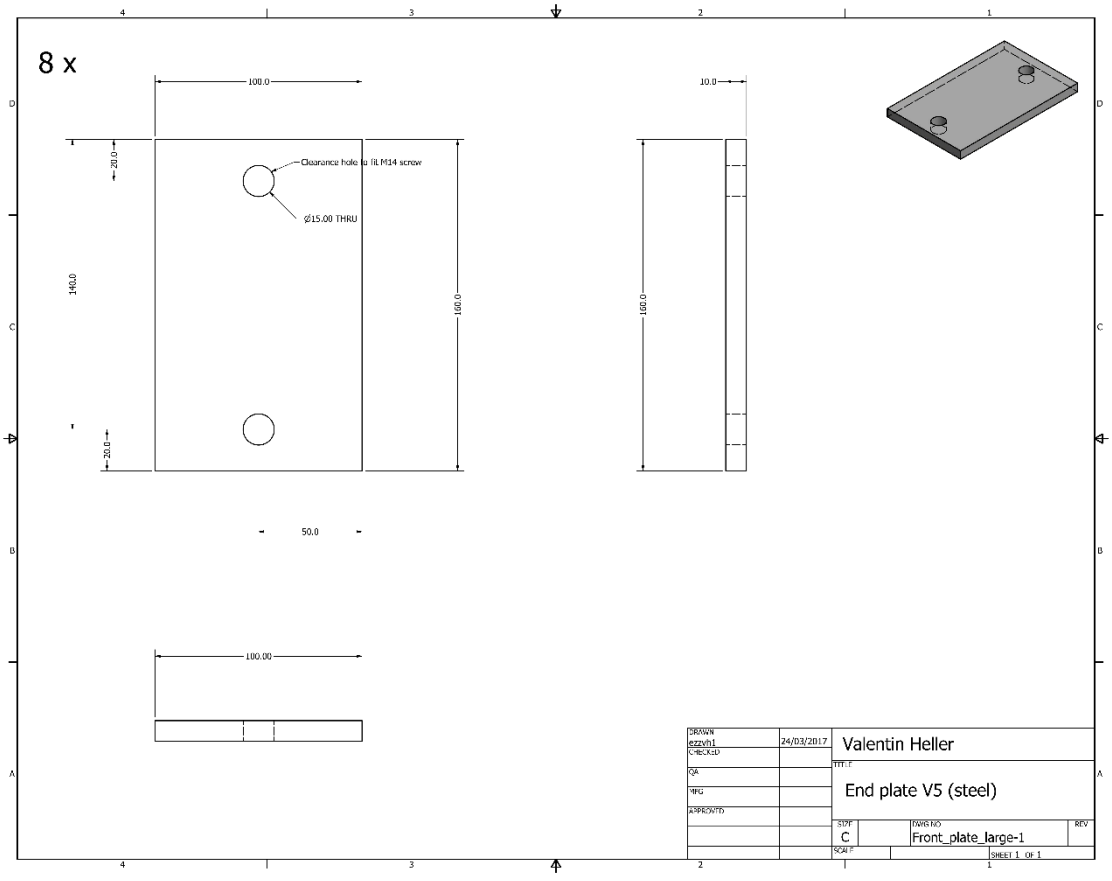
8 x
100.0
10.0
20.0
Clearance hole to fit M14 screw
Ø15.00 THRU
140.0
160.0
160.0
20.0
50.0
100.00
DRAWN
ezzvh1
24/03/2017
Valentin Heller
CHECKED
QA
MFG
APPROVED
TITLE
End plate V5 (steel)
SIZE
C
DWG NO
Front_plate_large-1
REV
SCALE
SHEET 1 OF 1

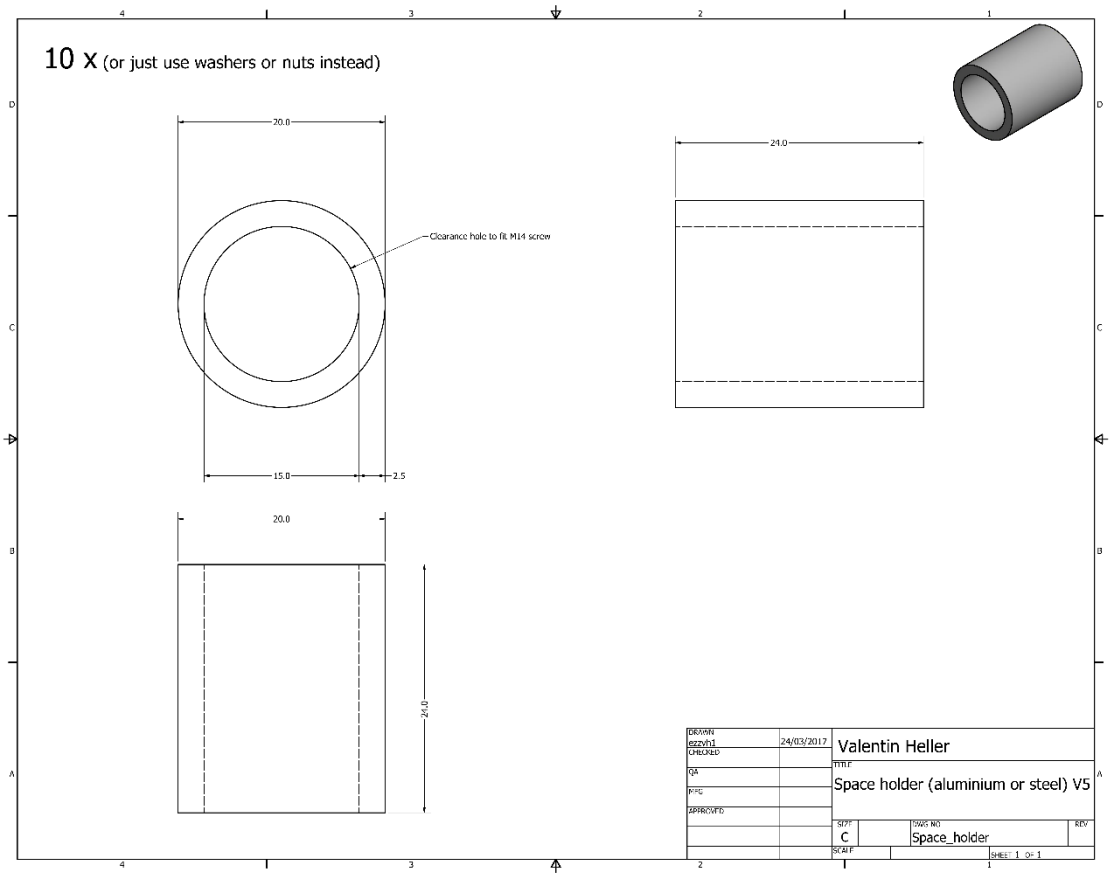
10 x (or just use washers or nuts instead)
20.0
Clearance hole to fit M14 screw
15.0
2.5
24.0
20.0
24.0
DRAWN
ezzvh1
24/03/2017
CHECKED
QA
MFG
APPROVED
Valentin Heller
TITLE
Space holder (aluminium or steel) V5
SIZE
C
DWG NO
Space_holder
REV
SCALE
SHEET 1 OF 1

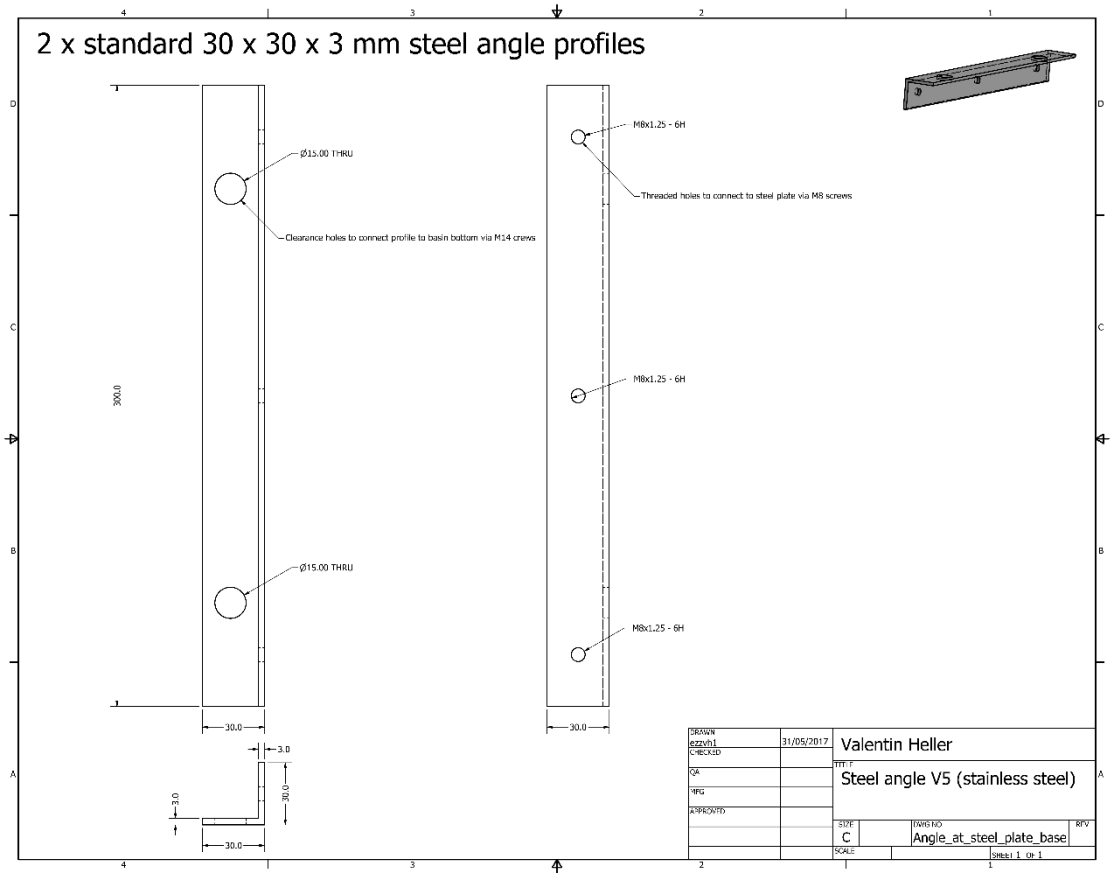
2 x standard 30 x 30 x 3 mm steel angle profiles
Ø15.00 THRU
Clearance holes to connect profile to basin bottom via M14 crews
300.0
Ø15.00 THRU
30.0
3.0
3.0
30.0
30.0
M8x1.25 - 6H
Threaded holes to connect to steel plate via M8 screws
M8x1.25 - 6H
M8x1.25 - 6H
30.0
DRAWN
ezzvh1
31/05/2017
CHECKED
QA
MFG
APPROVED
Valentin Heller
TITLE
Steel angle V5 (stainless steel)
SIZE
C
DWG NO
Angle_at_steel_plate_base
REV
SCALE
SHEET 1 OF 1

For illustrative purposes only

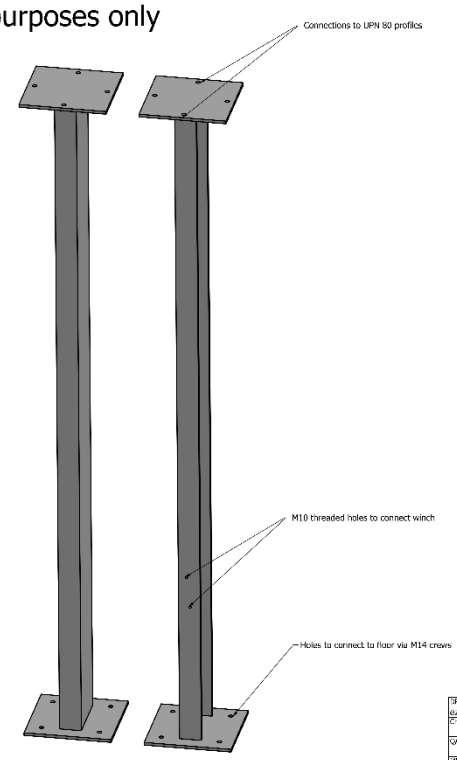


| | | |
|---|---|---|
| DRAWN ezzvh1 | 31/05/2017 | Valentin Heller |
| CHECKED | | |
| QA | | TITLE: Assembly support structure outside basin V5 |
| MFG | | |
| APPROVED | | SIZE: C / DWG NO: Assembly_support_structure / REV |
| | | SCALE / SHEET 1 OF 1 |

2 x steel plates (end plates of UPN 200 profile at top)

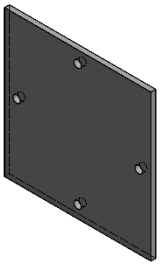

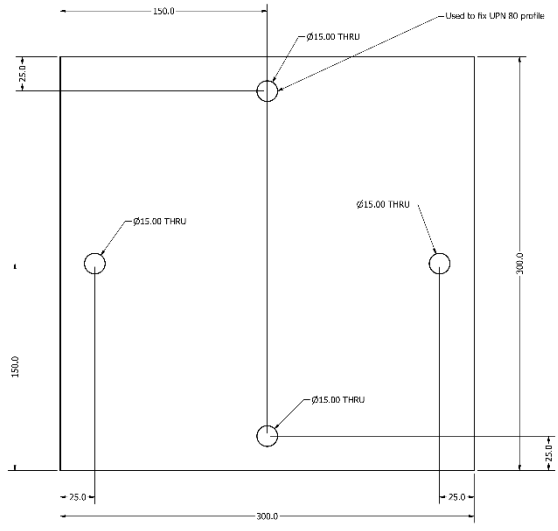



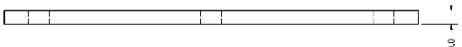


| | | |
|---|---|---|
| DRAWN ezzvh1 | 30/05/2017 | Valentin Heller |
| CHECKED | | |
| QA | | TITLE: End plates of UPN 200 profile top V5 (steel) |
| MFG | | |
| APPROVED | | SIZE: C / DWG NO: End_plate_support_top / REV |
| | | SCALE / SHEET 1 OF 1 |

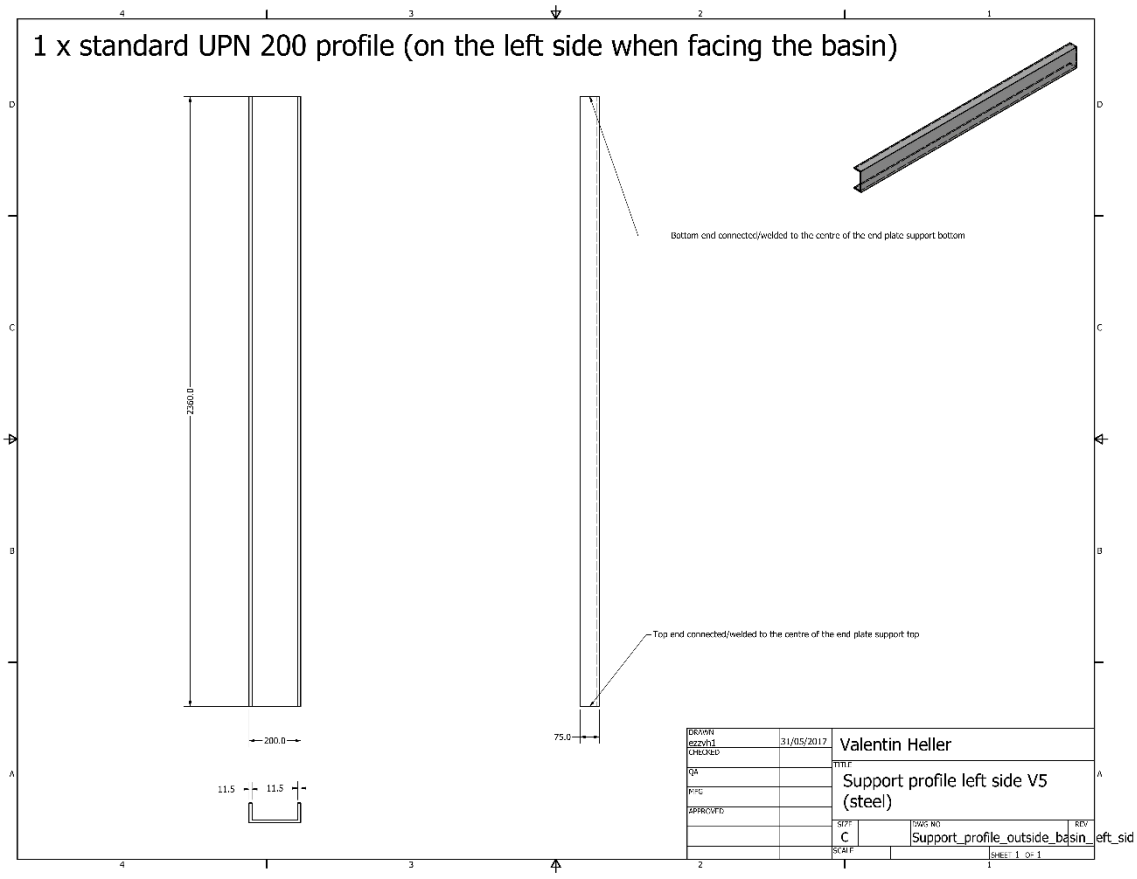
1 x standard UPN 200 profile (on the left side when facing the basin)
2360.0
200.0
11.5
11.5
75.0
Bottom end connected/welded to the centre of the end plate support bottom
Top end connected/welded to the centre of the end plate support top
DRAWN
ezzvh1
31/05/2017
CHECKED
QA
MFG
APPROVED
Valentin Heller
TITLE
Support profile left side V5 (steel)
SIZE
C
DWG NO
Support_profile_outside_basin_left_sid
REV
SCALE
SHEET 1 OF 1

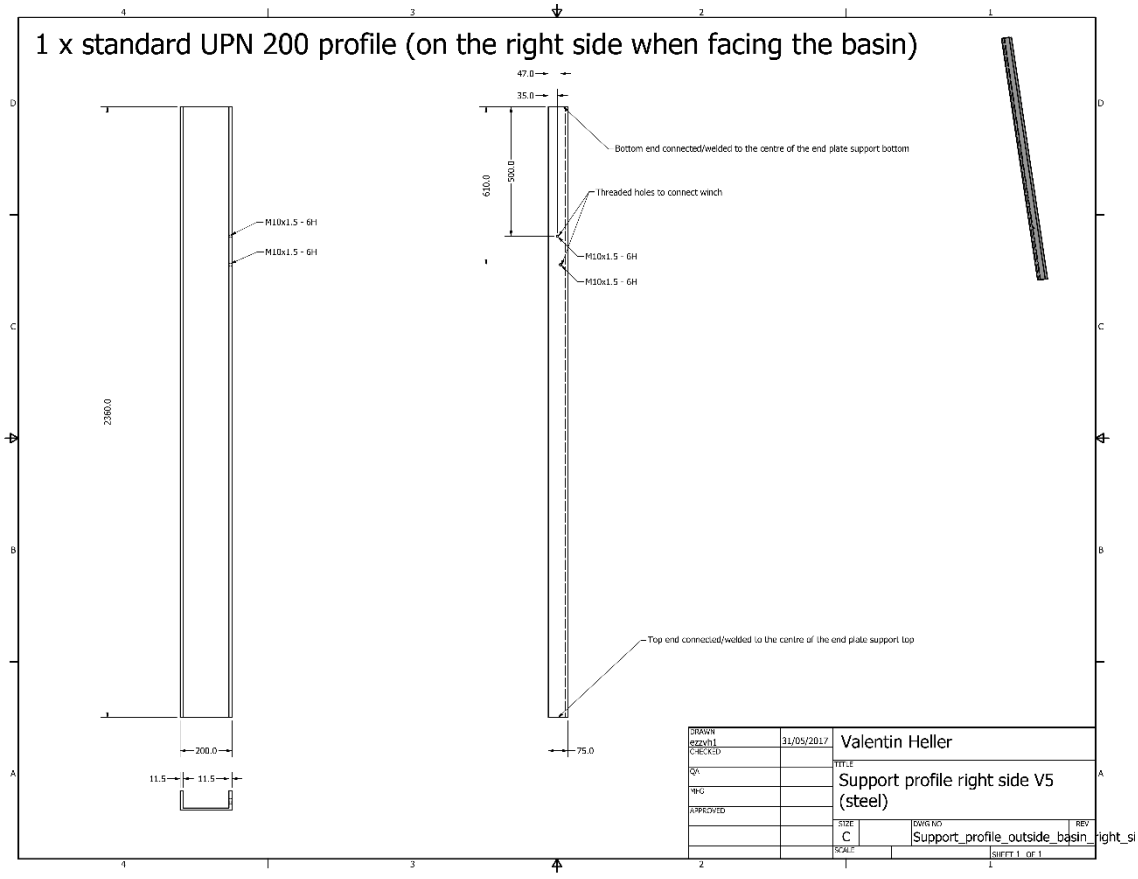
1 x standard UPN 200 profile (on the right side when facing the basin)
47.0
35.0
610.0
500.0
M10x1.5 - 6H
M10x1.5 - 6H
M10x1.5 - 6H
M10x1.5 - 6H
Threaded holes to connect winch
Bottom end connected/welded to the centre of the end plate support bottom
Top end connected/welded to the centre of the end plate support top
2360.0
200.0
11.5
11.5
75.0
DRAWN
ezzvh1
31/05/2017
CHECKED
QA
MFG
APPROVED
Valentin Heller
TITLE
Support profile right side V5 (steel)
SIZE
C
DWG NO
Support_profile_outside_basin_right_si
REV
SCALE
SHEET 1 OF 1

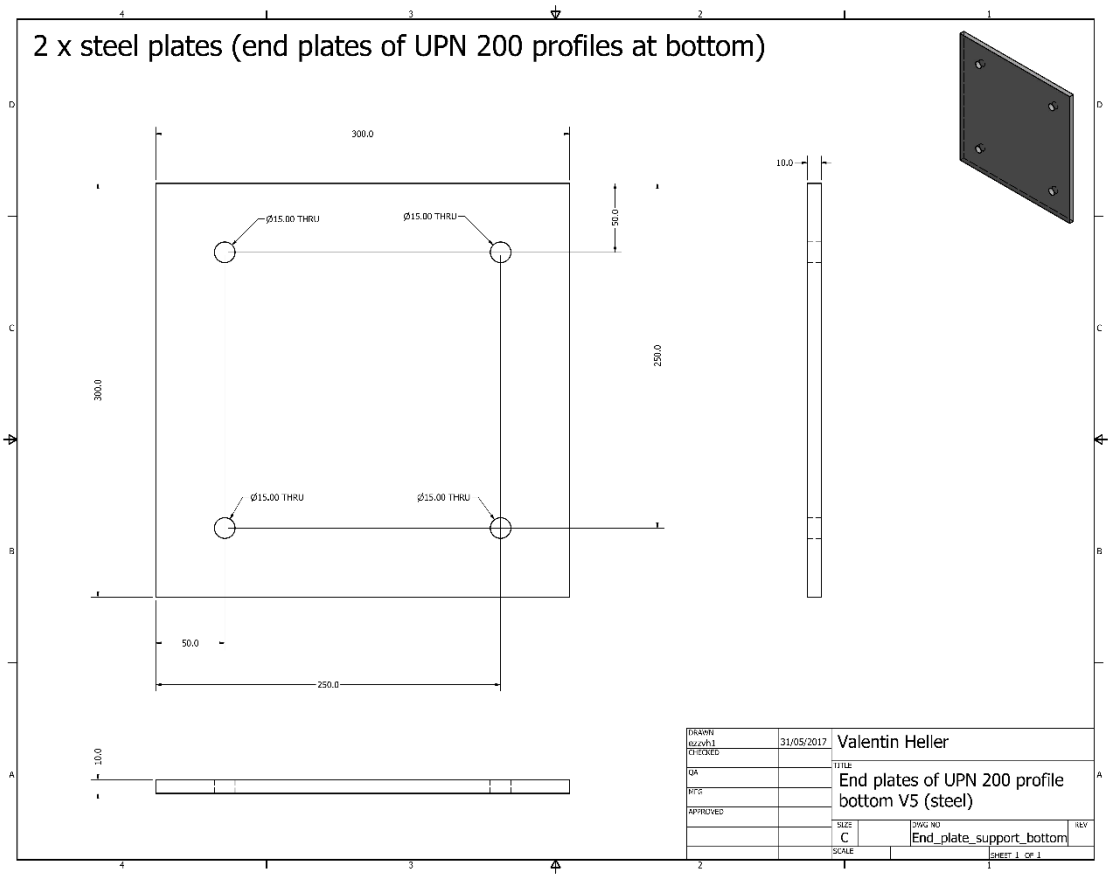
2 x steel plates (end plates of UPN 200 profiles at bottom)
300.0
Ø15.00 THRU
Ø15.00 THRU
50.0
250.0
300.0
Ø15.00 THRU
Ø15.00 THRU
50.0
250.0
10.0
10.0
DRAWN
ezzvh1
31/05/2017
Valentin Heller
CHECKED
QA
MFG
APPROVED
TITLE
End plates of UPN 200 profile bottom V5 (steel)
SIZE
C
DWG NO
End_plate_support_bottom
REV
SCALE
SHEET 1 OF 1

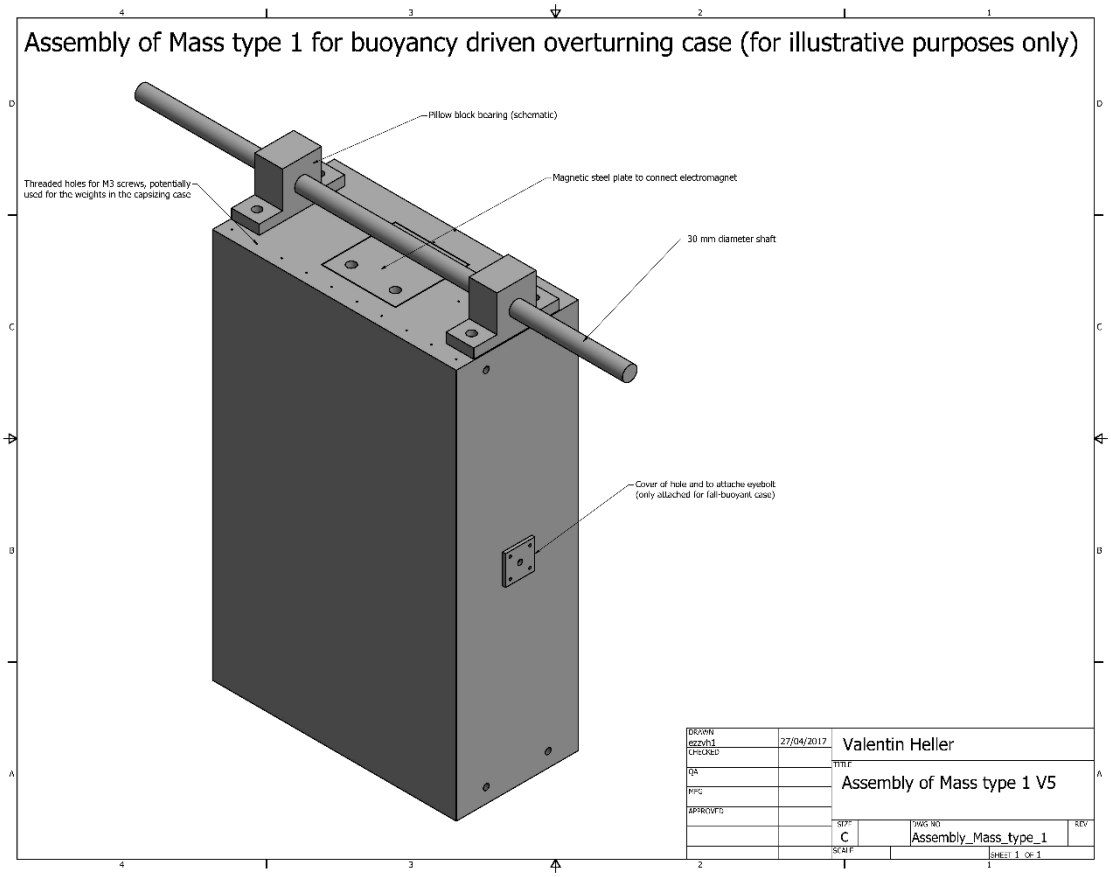
Assembly of Mass type 1 for buoyancy driven overturning case (for illustrative purposes only)
Pillow block bearing (schematic)
Threaded holes for M3 screws, potentially used for the weights in the capsizing case
Magnetic steel plate to connect electromagnet
30 mm diameter shaft
Cover of hole and to attache eyebolt (only attached for fall-buoyant case)
DRAWN
ezzvh1
27/04/2017
Valentin Heller
CHECKED
QA
MFG
APPROVED
TITLE
Assembly of Mass type 1 V5
SIZE
C
DWG NO
Assembly_Mass_type_1
REV
SCALE
SHEET 1 OF 1

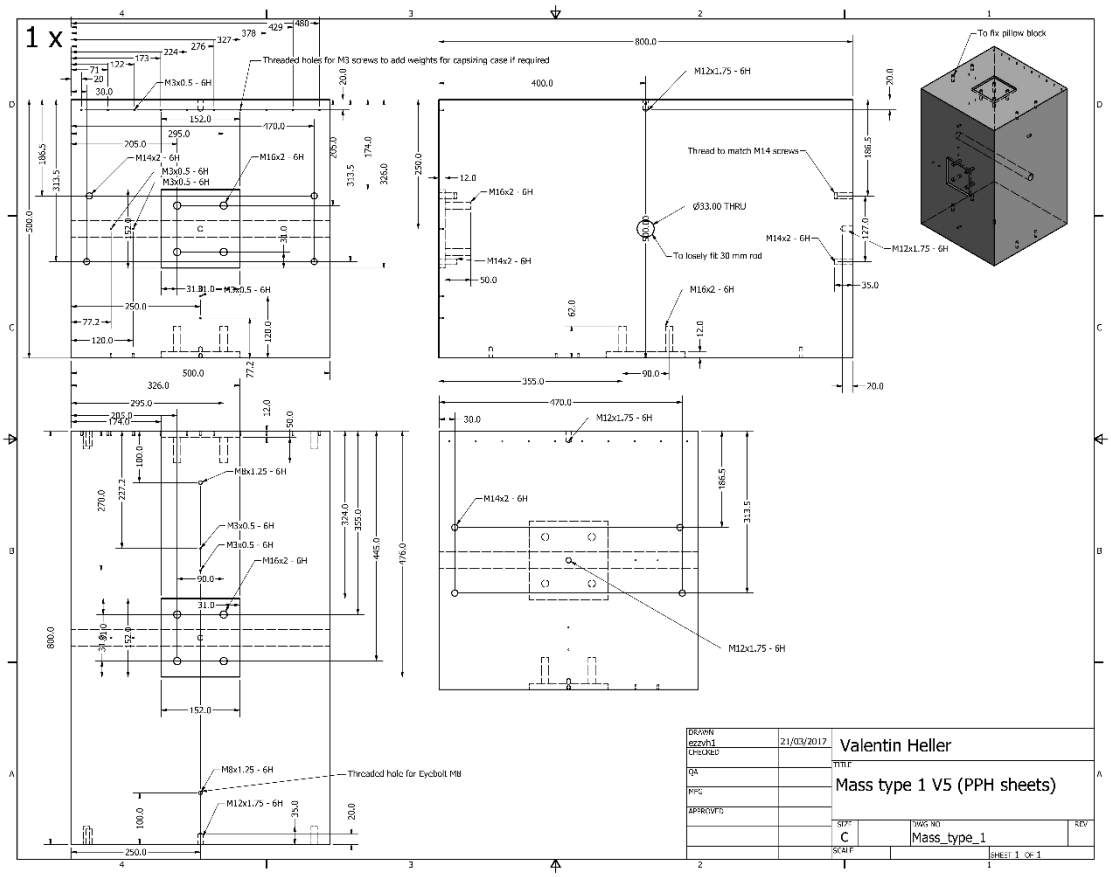
1 x
Threaded holes for M3 screws to add weights for capsizing case if required
M3x0.5 - 6H
M14x2 - 6H
M16x2 - 6H
M12x1.75 - 6H
Thread to match M14 screws
Ø33.00 THRU
To losely fit 30 mm rod
To fix pillow block
M8x1.25 - 6H
Threaded hole for Eyebolt M8
DRAWN ezzvh1
21/03/2017
Valentin Heller
CHECKED
QA
MFG
APPROVED
TITLE
Mass type 1 V5 (PPH sheets)
SIZE C
DWG NO Mass_type_1
REV
SCALE
SHEET 1 OF 1

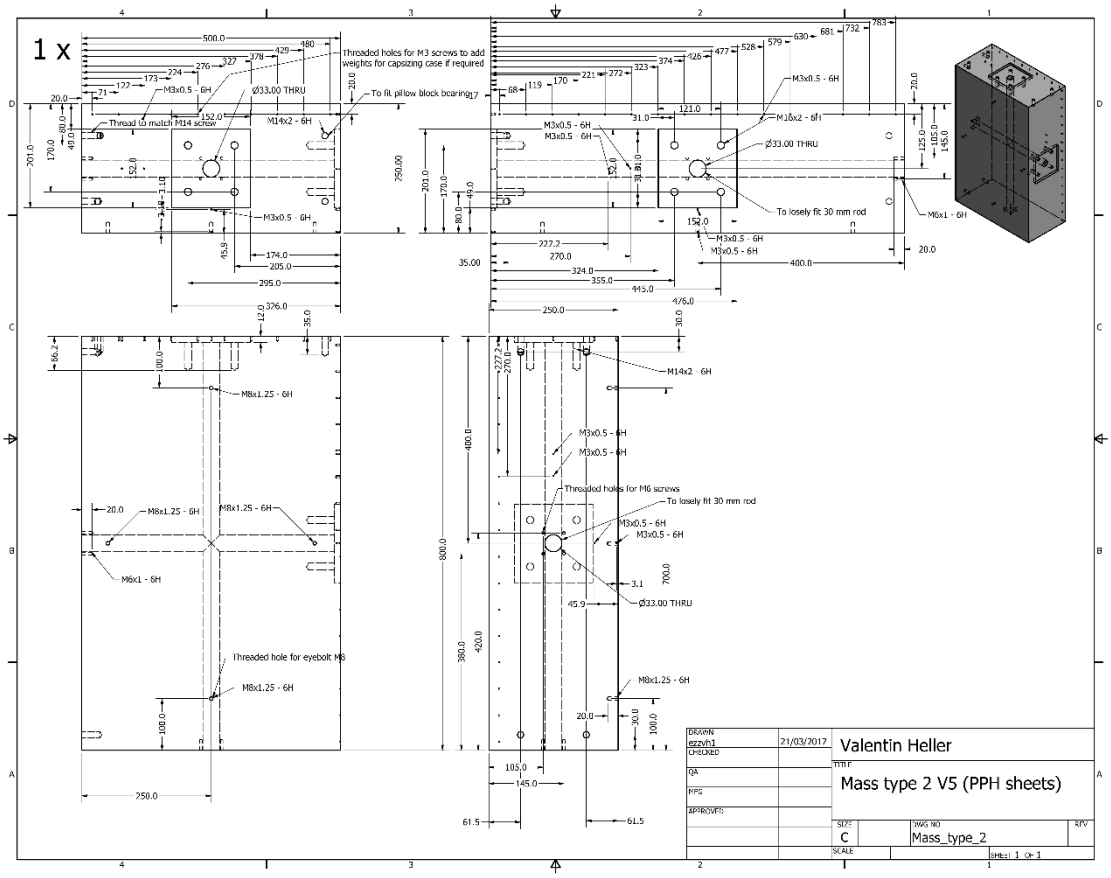
1 x
Threaded holes for M3 screws to add weights for capsizing case if required
To fit pillow block bearing
Thread to match M14 screw
Ø33.00 THRU
M3x0.5 - 6H
M14x2 - 6H
M16x2 - 6H
To losely fit 30 mm rod
M6x1 - 6H
M8x1.25 - 6H
Threaded holes for M6 screws
Threaded hole for eyebolt M8
DRAWN ezzvh1
21/03/2017
Valentin Heller
CHECKED
QA
MFG
APPROVED
TITLE
Mass type 2 V5 (PPH sheets)
SIZE C
DWG NO Mass_type_2
REV
SCALE
SHEET 1 OF 1

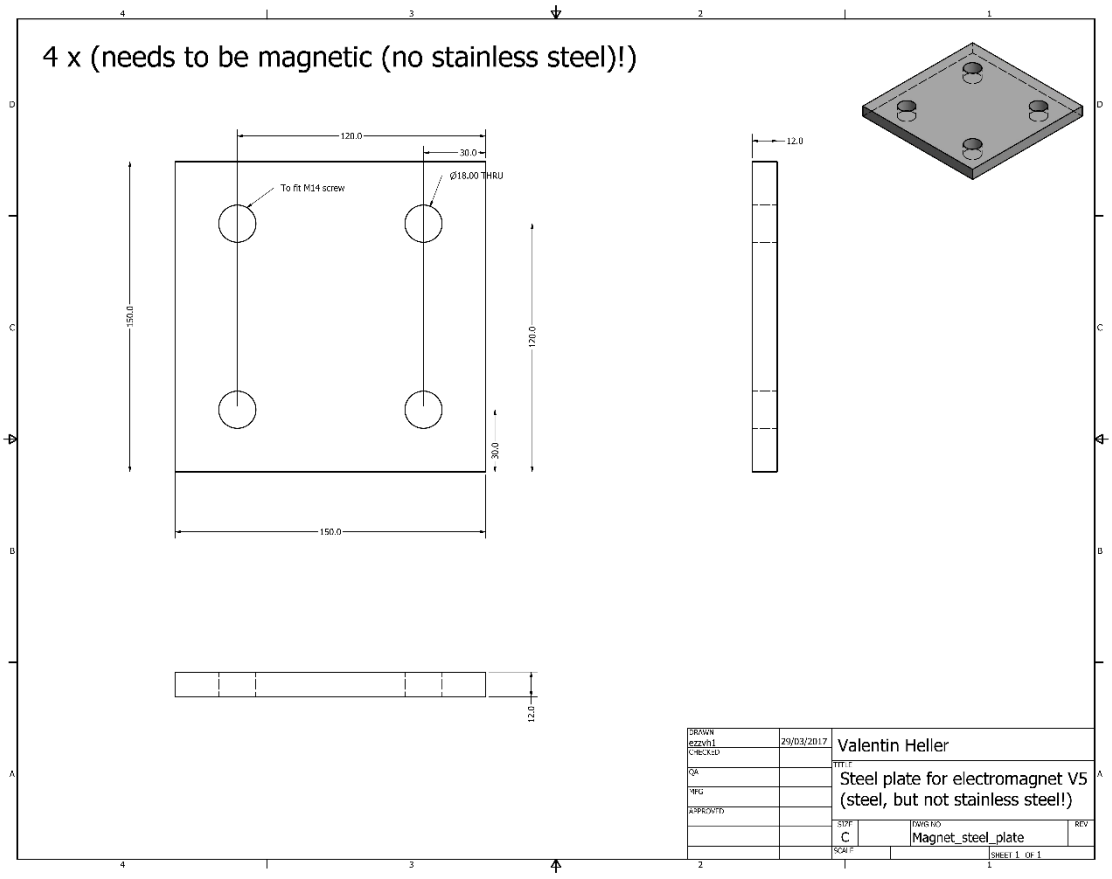
4 x (needs to be magnetic (no stainless steel)!)
120.0
30.0
To fit M14 screw
Ø18.00 THRU
150.0
120.0
30.0
150.0
12.0
12.0
DRAWN
ezzvh1
29/03/2017
Valentin Heller
CHECKED
QA
MFG
APPROVED
TITLE
Steel plate for electromagnet V5 (steel, but not stainless steel!)
SIZE
C
DWG NO
Magnet_steel_plate
REV
SCALE
SHEET 1 OF 1

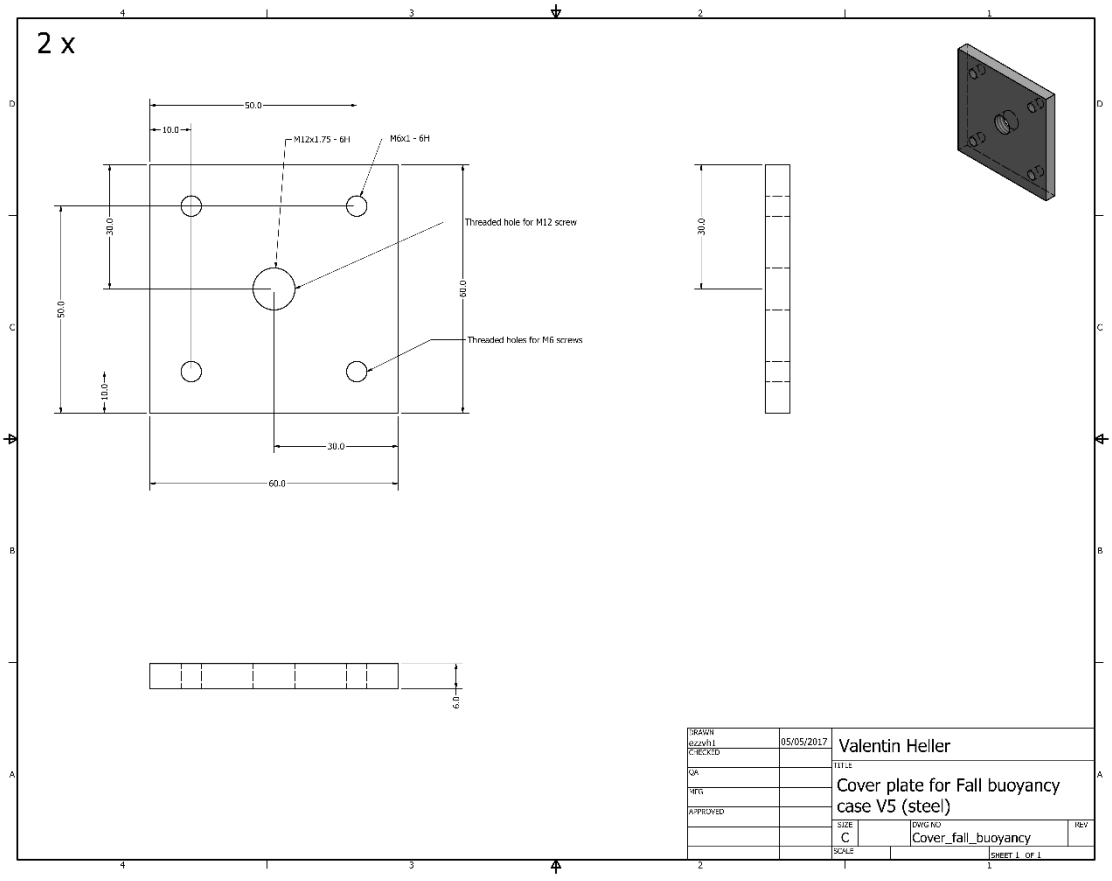
2 x
50.0
10.0
M12x1.75 - 6H
M6x1 - 6H
Threaded hole for M12 screw
Threaded holes for M6 screws
30.0
50.0
10.0
30.0
60.0
30.0
6.0
DRAWN
ezzvh1
05/05/2017
Valentin Heller
CHECKED
QA
MFG
APPROVED
TITLE
Cover plate for Fall buoyancy case V5 (steel)
SIZE
C
DWG NO
Cover_fall_buoyancy
REV
SCALE
SHEET 1 OF 1

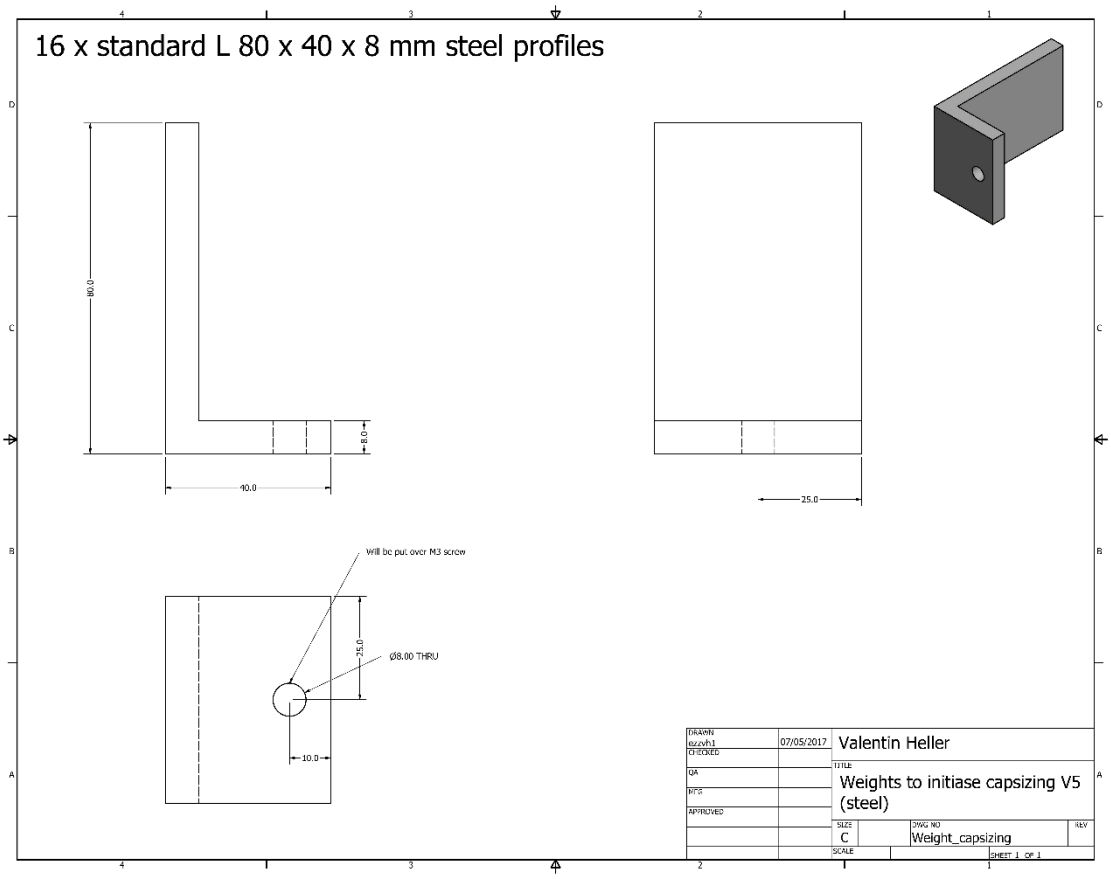
16 x standard L 80 x 40 x 8 mm steel profiles
80.0
8.0
40.0
25.0
Will be put over M3 screw
Ø8.00 THRU
25.0
10.0
DRAWN ezzvh1 07/05/2017 Valentin Heller
CHECKED
QA
MFG
APPROVED
TITLE
Weights to initiase capsizing V5 (steel)
SIZE C
DWG NO Weight_capsizing
REV
SCALE
SHEET 1 OF 1

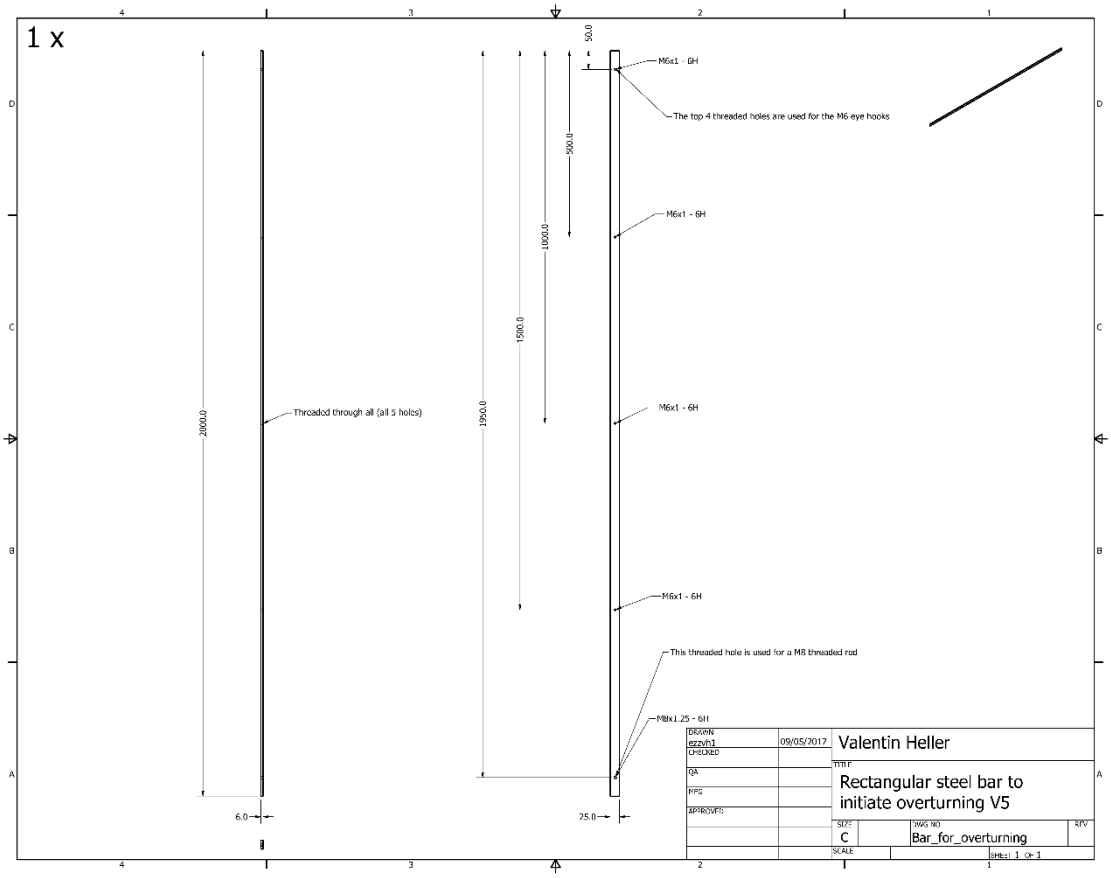
1 x
50.0
M6x1 - 6H
The top 4 threaded holes are used for the M6 eye hooks
500.0
M6x1 - 6H
1000.0
1500.0
1950.0
2000.0
Threaded through all (all 5 holes)
M6x1 - 6H
M6x1 - 6H
This threaded hole is used for a M8 threaded rod
M8x1.25 - 6H
6.0
25.0
DRAWN ezzvh1 09/05/2017 Valentin Heller
CHECKED
QA
MFG
APPROVED
TITLE
Rectangular steel bar to initiate overturning V5
SIZE C
DWG NO Bar_for_overturning
REV
SCALE
SHEET 1 OF 1